The role of matrix-oriented salt-bridge on the proton transport in a multimeric uncoupling protein 2

Afshan Ardalan[1], Stephanie O. Uwumarenogie[1], Michael Fish[1,2], Shahin Sowlati-Hashjin[3], Mikko Karttunen[3,4], Matthew D. Smith[2], and Masoud Jelokhani-Niaraki[1]*

[1] Department of Chemistry and Biochemistry, Wilfrid Laurier University, Waterloo, ON, Canada N2L 3C5; [2] Department of Biology, Wilfrid Laurier University, Waterloo, ON, Canada N2L 3C5; [3] Department of Chemistry, Western University, London, ON, Canada N6A 5B7; [4] Department of Applied Mathematics, Western University, London, ON, Canada N6A 5B7

Running title: Matrix salt-bridge network controls multimeric UCP2 function

* To whom correspondence should be addressed: Masoud Jelokhani-Niaraki: Department of Chemistry and Biochemistry, Wilfrid Laurier University, Waterloo, ON, Canada N2L 3C5; mjelokhani@wlu.ca; Tel. 519-884-0710 ext. 2284

Keywords: circular dichroism, fluorescence, membrane protein, protein self-assembly, proton transport, structure-function relationship, uncoupling proteins

Abstract

Uncoupling proteins (UCP[1]s) are members of the mitochondrial carrier superfamily (MCF) that transport protons across the inner mitochondrial membrane, thereby uncoupling respiration from ATP synthesis. The proton transport mechanism in UCPs is not fully understood. It has been suggested that members of MCF possess matrix and cytoplasmic salt-bridge networks, which could control substrate transport via alternative conformational changes. In the current study the role of the matrix-facing salt-bridge network in proton transport function of UCP2 and its molecular state in membranes were analyzed. The role of the matrix network was evaluated by introducing single and double mutations of positively-charged lysine residues (K38Q, K141Q, K239Q, and K38Q/K239Q) into UCP2. Proteins were expressed in *E. coli* membranes and reconstituted in phosphatidylcholine vesicles. CD spectroscopy and fluorescence methods were employed to characterize protein structure and function, respectively. Proton transport was significantly increased in single mutants compared to the wild-type protein but did not change significantly in the double mutant, suggesting a regulatory role for the matrix network. Monomeric UCP2 self-associated into a tetrameric functional form after reconstitution in lipid vesicles. This result was further supported by molecular dynamics (MD) simulations. The molecular forms of UCP2 in liposomes were also compared to those of another conformationally relevant protein, ADP/ATP carrier. In contrast to UCP2, ADP/ATP carrier did not form tetramers in lipid membranes. Overall, tetrameric forms of UCP2 transported protons in lipid membranes and this transport was regulated by the matrix salt-bridge network.

[1] AAC1, mitochondrial ADP/ATP carrier protein; C_8E_4, tetraethylene glycol monooctyl ether; IMM, inner mitochondrial membrane; IMS, mitochondrial intermembrane space; LDAO, n-dodecyl-N,N-Dimethylamine-N-oxide; MCF, mitochondrial carrier superfamily; MD, molecular dynamics; OG, octylglucopyranoside; PA, phosphatidic acid; PC, phosphatidylcholine; PCA, principal component analysis, PelB, pectate lyase B; PI, Phosphatidylinositol; POPC, 1-palmitoyl-2-oleoylphosphatidylcholine; RMSD, root mean square deviation; RMSF, root mean square fluctuation; ROS, reactive oxygen species; SASA, solvent accessible surface area; SPQ, 6-methoxy-N-(3-sulfopropyl)quinolinium; TEA, tetraethylammonium; TES, N-[tris(hydroxymethyl)methyl]-2-aminoethane-sulfonic acid; UCP, uncoupling protein.

INTRODUCTION

Uncoupling proteins (UCPs) form a subfamily within the mitochondrial anion carrier superfamily (MCF), located in the inner membrane of mitochondria (IMM) (1). UCPs attenuate proton motive force by providing a back-flux route for protons to move from the intermembrane space (IMS) to the matrix (2); proton motive force can control substrate pressure and cristae morphology in mitochondria (2).

Five homologues of human UCPs have been discovered to date (UCPs1-5). All five homologues transport proton and anions and possess comparable helical conformations (3). Among these, UCPs 2, 4 and 5 are mainly found in the human central nervous system and are known as neuronal UCPs (4). UCPs 2, 4 and 5 share 59%, 30% and 33% sequence identity with the prototypic UCP1, respectively (1). UCP2 is unique among other UCPs for its ubiquitous expression pattern (5).

The wide distribution of UCP2 in various tissues signifies its potential multiple roles in physiological or pathological conditions (6). The role of UCP2 in decreasing mitochondrial ROS concentration has been shown in several studies (7-9). Other studies have revealed a remarkable up-regulation of UCP2 expression in different types of cancer including tumor growth in neck, head, skin, prostate, colon and breast (10-13). UCP2 overexpression can also result in inhibition of cytochrome C release and reduction of caspase 9 activity in lung adenocarcinoma cells, thereby showing antiapoptotic effects (14). These antiapoptotic properties of UCP2 have been attributed to its inhibitory effect in excessive ROS accumulation (14). It has been also speculated that distortions in expression and regulation of UCP2 could be among the causes of aging, type 2 diabetes, obesity and heart failure (5).

Although proton transport activity is a common function of all UCPs, its detailed mechanism is not yet fully understood. Different studies have shed light on several aspects of the proton transport mechanism and functional structure of UCPs. Despite inconsistencies, all agree that proton flux through UCPs is activated by fatty acids and inhibited by purine nucleotides (3). Proposed mechanisms of UCP activation by fatty acids can be summarized in three models: the fatty acid cycling model (15), the buffering/cofactor model (16), and the long-chain fatty acid shuttling model (17). In the fatty acid cycling model, protonated fatty acids that reside in the IMS "flip-flop" across the IMM and release their proton into the matrix. The fatty acid anion is then transported from the matrix to the IMS by UCP (15). In the buffering model, a translocon channel is involved. Fatty acid anions bind to UCP, accept and transport protons via their carboxylate group to the buffering amino acids of the protein, one by one, all the way to the matrix side through the translocon channel (1,16). The shuttling model proposes that fatty acid carboxylate heads move across the IMM toward the IMS and matrix, thereby getting protonated in the IMS and releasing their protons in the matrix, while remaining bound to the protein (17).

None of thee above models is universally accepted, and there is experimental evidence that either supports or opposes each model (1). In addition, as membrane proteins have always been challenging to isolate and purify in their native functional forms, in some cases it is difficult to reach consensus regarding the molecularity of their functional structure. In the case of UCPs, there have been discrepancies about the molecularity of the active proteins in the membrane; monomeric (18), dimeric (19) and tetrameric forms have been all reported as the functional forms of UCPs (3).

Being a subfamily of the MCF superfamily, UCPs share distinct structural similarities with AAC1, for which there is a known crystal structure (1,20). The NMR structure of UCP2 confirms its remarkable similarities with the AAC1 protein (21). It is noteworthy that all members of the MCF superfamily contain a trilateral structure that includes 3 tandem repeats. Each repeat is comprised of about 100 amino acids folded into two transmembrane α-helices and are connected by a hydrophilic loop, positioned toward the matrix side of the mitochondrion (2,21). Also, two types of conserved motifs are found at the water-accessible interfaces of MCF proteins. Firstly, the signature motif PX[D/E]XX[R/K] located on odd-numbered helices (1,3 and 5) close to the matrix, and secondly, [F/Y][D/E]XX[R/K] motifs located on even-numbered helices (2,4 and 6) close to the IMS (22). These conserved motifs on both sides form salt-bridge networks, which could dictate the protein's functional conformation via successive disruptions and reformations of the salt-bridges.

Generally, the transport mechanism in MCF proteins could thereby be controlled by alternating conformational switches of the protein from cytoplasmic state (in which the substrate binding site is exposed the IMS) to matrix state (in which the substrate binding site is exposed the matrix) in response to substrate binding (22).

Factors determining the rate of proton transport in UCP2 are yet to be determined; however, using point mutations, an inverse relationship between the rate of proton transport of UCP2 and the density of the transmembrane helix packing in the monomeric UCP has been reported previously (23). Mutations which led to more relaxed conformations (less dense packing due to weaker interactions between transmembrane helices) showed higher proton transport rates (23). UCP2 carries an overall positive charge of +15, which is mostly due to the presence of basic residues located close the matrix side of the protein (23). Studies have suggested that the matrix side electrostatic properties can have an important role in attraction and accumulation of anions which might affect the local conformation of the protein and transport rate of ions (23,24).

In order to further investigate the mechanism of proton transport in UCP2 and understand the role of the matrix side salt-bridge network and its electrostatic features on proton transport, in this study four mutants have been prepared containing point mutations. Salt-bridges were disrupted one/two at a time by eliminating the positively charged lysine residues found in the above-mentioned signature motifs on transmembrane helices 1, 3 and 5 (Lys → Gln mutations) (Figure 1 and S1). UCP2 and its mutants were expressed in *E. coli* membranes, then purified and reconstituted in lipid vesicles for proton transport, transport inhibition, as well as spectroscopic conformational analyses. Our results suggest that the matrix side salt-bridge network could have a regulatory effect on the proton transport mechanism of UCP2. We have also investigated the quaternary structures of UCP2 and its mutants in detergents and lipid membranes; and showed that the associated tetrameric UCP2 can transport protons across lipid bilayers. These structures were compared to those of AAC1 (PDB id 1OKC). Overall, this study contributes to the understanding of the mechanism of proton transport and the role of the matrix salt-bridge network in UCP2.

RESULTS

Expression and purification of UCP2, its mutants and AAC1

In order to study the role of the matrix salt-bridge network on the proton transport rate of UCP2, three single mutants (K38Q, K141Q, K239Q) and one double mutant (K38Q/K239Q) form of the protein were generated (Figure S1). Glutamine was chosen for its lack of positive charge and its relative structural similarity with lysine. One salt-bridge was disrupted in single mutants and two salt-bridges were disrupted in the double mutant. The cDNAs of the mutants were cloned into pET26b(+) and expressed in *E. coli* BL21 CD+ cells using the auto-induction method (25). Cloning the cDNAs of UCP2 and its mutants into pET26b (+) also resulted the pelB signal peptide being added to the N-terminus of the proteins, which targets UCPs to the *E. coli* inner membrane (3). The pelB signal peptide normally directs secreted proteins to the periplasmic space; however, the transmembrane segments of UCP2 prevent full translocation and lead to insertion into the membrane due to hydrophobic interactions with bacterial membrane (3,26). His-tagged proteins were purified on nickel-containing columns and their purity was confirmed by SDS-PAGE (Figure 2a). Bands around 33, 66 and 132 kDa were observed for all of the proteins on the polyacrylamide gel. Furthermore, Western Blot analysis using an α-UCP1,2,3 antibody reacted with all three bands (Figure 2b) suggesting that they correlate with monomeric, dimeric and tetrameric forms of UCP2 and its mutants, respectively, as has been observed previously (3). The monomeric and dimeric states of AAC1 were also detected by Western Blot analysis (Figure S2).

The role of matrix salt-bridge network and conformation on proton transport function of UCP2

To compare the proton transport rates of UCP2 and the mutants, proteins were reconstituted into egg yolk PC (~60% PC) vesicles. Proton transport rates were studied using a fluorescence quenching assay, as described previously (Figure S3) (24). All proteins were only able to transport

protons after addition of PA (phosphatidic acid). This is consistent with previously reported data on the inability of UCP1 (in proteoliposome systems and mitoplasts) to transport protons in the absence of fatty acids (27,28). Table 1 and the blue bars in Figure 3a exhibit the proton transport rates of UCP2 and its four mutants. The rate at which UCP2 transported protons was 2.43 ± 0.16 μmol/min/mg protein, which is equal to 1–2 protons per molecule of UCP2 per second. This result is within the range of previously reported proton transport rates for reconstituted recombinant UCP2 in vesicles (3,24). Our results showed that all single mutants transported protons across the bilayer at rates which were significantly ($p<0.05$) higher than UCP2. All single mutants showed a minimum two-fold increase in proton transport rate compared to the wild-type protein. The double mutant (K38Q/K239Q) transported protons four times slower than each of the related single mutants (K38Q and K239Q). However, no significant difference was observed between the proton transport rates of the double mutant and UCP2. Comparison of proton transport rates among UCP2 and its single mutants implies a regulatory role for the matrix salt-bridge network on proton transport.

The inhibitory role of ATP on proton transport rates of UCP2 and its mutants was also investigated. Proteoliposomes were incubated with 500 μM ATP for 2 minutes prior to measurement. The results are shown in Table 1 and Figures 3a and 3b. Incubation of the proteoliposomes with ATP resulted in a 50 – 80% decrease in the rate of proton transport. ATP inhibition was about 72% for UCP2, which is comparable with previously reported results (29). Partial inhibition of reconstituted UCPs by ATP has been reported previously (24), and it has been also shown that ATP affinity to UCPs decreases drastically upon increasing pH (24,28). It is suggested that the addition of H^+ could result in the breakage of the "gate keeper" salt-bridges (by protonating aspartate and glutamate) that block the entrance of nucleotide binding cavity, thus allowing the nucleotides to access the binding cavity to bind to the protein (30). Mutation of lysine 141 and lysine 239 to glutamine (Figure S1) resulted in a decrease (~20%) in inhibitory effect of ATP, compared to UCP2, which in turn implies a role for these two residues in interacting with the nucleotide.

The SDS-PAGE analyses of these protein samples are shown in Figure 2a. All proteins are mixtures of monomeric and multimeric forms, and exhibit molecular masses characteristic of monomeric, dimeric and tetrameric species, which were further characterized and verified by Western Blot analysis (Figure 2b).

Conformational characteristics of UCP2 and its mutants in OG detergent were analyzed using CD spectroscopy. The CD spectra of the proteins (Figure 4) exhibited two negative maxima at 208 nm and 222 nm, as well as a positive maximum around 193 nm (close to two times in intensity compared to the negative maxima; not shown). Together, these spectral features are typical of a helical backbone secondary structure of proteins, correlated to $\pi \rightarrow \pi^*$ and $n \rightarrow \pi^*$ transitions in the peptide bond (31). Furthermore, the ellipticity ratio ($\theta_{208}/\theta_{222}$) was in the range of 0.9-1.0 for all five spectra, typical of largely α helical protein structures (32). Despite sharing the helical conformation, slight differences in the negative maxima intensity (~30% more negative in UCP2) can be observed between the spectra of UCP2 and the mutants K38Q, K239Q, and K38Q/K239Q, which indicates a higher helical content in UCP2 in comparison to these mutants. On the other hand, the spectrum related to K141Q is the closest to UCP2. These conformations of UCP2 and its mutants exhibit structural similarities indicating that mutations have not altered the overall conformation of the protein. This observation was further supported by the proton transport ability of the mutants (Table 1; Figure 3). Nevertheless, the possibility of local structural alterations cannot be excluded. These local changes could not be revealed in the far-UV range of the CD spectra, which generally gives information about the average backbone conformation of proteins.

Multimeriztion of UCP2 in lipid vesicles

As previously shown, UCP2 and its mutants existed as a mix of monomeric, dimeric and tetrameric forms in OG detergent (Figures 2a and 2b). Once UCP2 and its mutants were reconstituted in lipid vesicles from detergent (see the Experimental Procedures section), the resulting proteoliposomes were analyzed using SDS-PAGE (Figure 5). Interestingly, as can be observed in Figure 5, it is apparent that all molecular forms of

UCP2 (and its mutants) associate to form a single multimeric (tetrameric) complex when reconstituted into liposomes.

To further investigate the spontaneous oligomerization of UCP2 in lipid, the protein was isolated from *E. coli* in its monomeric form in OG detergent. The pure UCP2 monomers were then reconstituted into lipid vesicles. The SDS-PAGE analysis of UCP2 before (in OG) and after reconstitution (in PC vesicles) is shown in Figure 6. The gel images of UCP2 show that, under our experimental conditions, reconstitution of UCP2 monomer (in OG) into PC vesicles resulted in spontaneous self-association of UCP2 into a single tetrameric molecular form (Figure 6, bottom). Under the same conditions, AAC1 did not form tetrameric complexes in lipids. Instead, it maintained its mix of monomeric and dimeric forms (in OG) when reconstituted into liposomes (Figure 5, lane 2; and Figure 6).

To characterize and compare the conformation of UCP2 monomer and AAC1 before (in OG) and after reconstitution into liposomes, samples were analyzed by CD spectroscopy (Figure 6). The CD spectra of the mixed molecular forms of UCP2 (monomer, dimer and tetramer) and AAC1 (monomer and dimer) in OG detergent exhibit comparable helical conformations (Figure 6, inset), which is expected based on the known similarities of the structures and co-presence of different monomeric and associated molecular forms in both proteins. In UCP2, the far-UV CD signal is notably enhanced after reconstitution of the monomer in liposomes, indicating a higher helical compared to that of protein in OG detergent (Figure 6). This drastic conformational change reveals the important role of the lipid environment in the folding of UCP2. In addition to their difference in signal intensity, the shape of the CD spectrum of UCP2 in proteoliposomes differs from that of the monomer in OG. Particularly, in vesicles, a shoulder-like $\pi \rightarrow \pi^*$ parallel polarized transition band around 208 nm replaces the minimum band in OG, and also a considerably more intense $n \rightarrow \pi^*$ transition band appears at 222 nm. The $\theta_{208}/\theta_{222}$ ellipticity ratio of the UCP2 monomer spectrum changed from 1.07 to 0.68 after reconstitution in liposomes (Figure 6). The $\theta_{208}/\theta_{222}$ ellipticity ratios lower than one have been previously reported for the UCP helical bundle motifs and self-associated proteins (3). Relative decrease in molar ellipticity at 208 nm (in comparison to ellipticity at 222 nm) and its red shift, due to intramolecular interaction between helical motifs and protein association, have been also reported for UCP1 and other membrane proteins (26,33-35). In comparison with UCP2, the negative ellipticity for AAC1 in liposomes is much less enhanced. The $\theta_{208}/\theta_{222}$ ellipticity ratio of AAC1 changed from 0.89 in OG detergent to 0.84 after reconstitution in liposomes, which is consistent with the protein adopting a similar conformation in these environments (mix of monomeric and dimeric forms) (Figure 6).

The differences between the CD spectra of reconstituted UCP2 and AAC1 show that the two proteins acquire different molecular forms after reconstitution in PC vesicles, under the same experimental conditions. In liposomes, both the considerably lower negative ellipticity and higher $\theta_{208}/\theta_{222}$ ellipticity ratio of AAC1 compared to UCP2 (0.84 vs. 0.68) are consistent with a lower degree of association in AAC1.

To confirm the functional equivalence of reconstituted proteins in different preparations (monomeric vs. mixed monomeric/multimeric), the proton transport of reconstituted monomeric UCP2 in liposomes was measured to be 2.14 ± 0.09 μmol/min/mg of protein. This value is comparable to the proton transport rate of the reconstituted mixed monomeric/multimeric UCP2 reported in Figure 3a and Table 1. As expected, AAC1 did not show considerable proton transport in comparison to UCP2 (data not shown).

In summary, our results from gel electrophoresis, CD spectroscopy and proton transport studies suggest that UCP2 and AAC1 act differently in liposomes. UCP2 monomers can associate into a functional tetrameric form in PC vesicles, while only monomeric and/or dimeric forms (but no tetrameric forms) were detectable for AAC1 in similar milieus.

MD simulations

To further evaluate our results, all-atom MD simulations were conducted on monomeric, dimeric, and tetrameric UCP2 in POPC model bilayers, which provided atomic-level details of protein-protein and protein-lipid interactions. Principal component analysis (PCA) of the proteins (Figure S4) indicate the different behaviors of

different UCP2 molecular states in the bilayer. The smaller average root mean square deviations (RMSDs) of the protein backbone and the root mean square fluctuations (RMSFs) of the protein C_α over the course of the simulation (Figures S5 and S6) suggest that in the POPC bilayer the monomeric and tetrameric UCP2 are structurally more stable than the dimeric form. The interactions of UCP2 monomeric units with one another, and with the lipid environment stabilize the multimers. Specifically, in the tetrameric state, salt-bridges are formed between the protein units on the intermembrane space and matrix sides of the proteins (Figure S7). Similar salt-bridges are also formed in the dimer (Figure S7). In addition to the salt-bridges in the tetrameric form, the hydrogen bonds (d(donor⋯acceptor) $\leq$ 0.35 nm and ∠(acceptor–donor–hydrogen) $\leq 30^\circ$) between the protein units (Figure S8) and between the protein and lipid (Figure S9) stabilize UCP2 in the POPC bilayer. On average 226, 436, and 872 hydrogen bonds between the helices (inter- and intra-helical) plus 32, 58, and 72 hydrogen bonds between the protein and the bilayer are formed in the monomeric, dimeric, and tetrameric forms of UCP2, respectively. Moreover, protein-protein and protein-lipid hydrophobic interactions (distance based) further stabilize all three molecular forms of the protein. Interestingly, formation of salt-bridges and other interactions does not warrant a protein dimeric structure as stable as those of monomeric and tetrameric forms, as reflected in the RMSD and RMSF plots (Figures S5 and S7).

The overall initial structure of UCP2 is maintained in all three forms (monomer, dimer, and tetramer) throughout the MD simulations. However, despite the general resemblance between the initial and final structures, there are subtle, yet notable changes that occur upon inserting the protein in the bilayer (Figures 7 and S4). Particularly, as is shown in Figure 7, all three forms of UCP2 shrink to some extent in the lipid bilayer. This contraction is also reflected in the radius of gyration (R_g) of the protein, which decreases with time (Figure S10). The shrinkage arises from the movement of TM α-helices toward each other when placed in a lipid bilayer, resulting in the adoption of a more packed structure to prevent/minimize the exposure of polar amino acid residues to the hydrophobic POPC tails and/or to the non-polar residues of the neighboring protein(s) (Figure 7). This observation is consistent with the gel electrophoresis data and the CD spectra, which also indicate self-association of the protein and more dense interaction of the helices in lipid bilayers (Figure 6). Figures S11 – S15 compare the final MD structures of UCP2 molecular forms with the initial structure. Other than the overall shrinkage, the most significant deviation from the initial structure of the protein in a lipid bilayer is observed in the case of the monomeric UCP2. Specifically, TM helix 5 (starting from residue 214) was shortened by approximately 2 turns during the simulation, elongating the linker between helices 4 and 5 (Figure S11).

Figures S12 and S13 indicate that dimeric and tetrameric UCP2 adopt asymmetric conformations (the deviations from the initial structure are not similar among their constituting units), which is also reflected in the PCA (Figure S4). This is also revealed by the average numbers of hydrogen bonds between the protein and the bilayer for the three UCP2 forms. Figures S14 and S15 provide a more detailed comparison between each unit of the multimeric UCP2 and the initial monomeric structure. Despite different patterns of change in the units, unlike the monomeric UCP2, TM helix 5 is not shortened in any of the multimeric forms. In agreement with a previous all-atom MD study of monomeric UCP2 (36), the solvent accessible surface area (SASA) of all three molecular forms UCP2 (Figure S16) are considerably reduced in the lipid bilayer compared to the initial structure (monomeric) in detergent micelles. Variation of protein SASAs in different environments is common and has been reported for a number of proteins (37-39). As is seen in Figure S16, SASA of the tetramer is smallest compared to the monomer and dimer, decreasing drastically during the first 20 ns and reaching a plateau after ~60 ns. The overall shape of the RMSD and RMSF plots (Figure S5 and S6), the smaller average SASA, and the fact that helix 5 is not shortened in the tetrameric form reflect the stability and potential existence of tetrameric UCP2 in lipid membranes.

Discussion

The matrix-facing salt-bridge network is a regulator of proton transport in UCP2

Comparing the fatty acid-dependent proton transport rates of UCP2 and its mutants suggests a regulatory role for the matrix salt-bridge network. Signature motifs PLDTAKV, PTDVVKV and PVDVVKT present on helices 1, 3, and 5, respectively, are involved in the UCP2 matrix-facing salt-bridge network (22). Under our experimental conditions, the low proton transport rates for UCP2 and its mutants were in better agreement with the behavior of a transporter/carrier as compared to an ion channel (27). However, the possibility of increased transport rates under different physicochemical and/or physiological conditions (such as larger potential differences across the mitochondrial membrane and interactions of other proteins in the mitochondrial inner-membrane) cannot be excluded. As shown in Figure 3a and Table 1, disruption of a single amino acid in the matrix-oriented salt-bridge resulted in an increase of more than two times in the proton transport rate of UCP2.

Combining the electrophoresis (Figure 2a and b), CD (Figure 4), and proton transport (Figure 3a and Table 1) analyses of UCP2 and its mutants reveals that the mutations did not have a substantial impact on the overall conformation, intramolecular helical packing and molecularity of the proteins in membrane-like environments (Figure 5). The differences in proton transport rates of UCP2 and the mutants can thus be attributed to the disruption of the salt-bridge network (inducing local conformational changes) rather than perturbing the overall tertiary structure of the proteins. Superposition of the energy-minimized structures of UCP2 and mutants [using Chimera software (40)], revealed that all 5 proteins form a network between the helices that are different in geometry (Figure S17). Our data suggest that the proton transport function of UCP2 can be attributed to the interplay between four different but correlated factors: (i) the electrostatic interactions between the amino acid side-chains involved in the matrix (and cytoplasmic) salt-bridge network(s); (ii) the geometry of the space between the transmembrane helices; (iii) the presence of positive charge at the fatty acid binding sites of the protein; and (iv) the synchronized interaction of the transmembrane helices leading to interconversion between the matrix state to the cytoplasmic (intermembrane) state and *vice versa*.

By comparing the proton transport rates of UCP2 and the point-mutants that were prepared for the current study, we can conclude that salt-bridge formation caused by electrostatic interaction between lysine and aspartate side-chain pairs generates a cumulative electric field, which can have a regulating/filtering effect on transporting protons and other ionic species, such as chloride (Figure 1). Disrupting any of these salt-bridges results in weakening/distorting this electrostatic filter. Each of the three single mutants of UCP2 (all include a Lys → Gln mutation) causes a change in the matrix salt-bridge network by eliminating the positive charge of lysine and freeing the negative charge of aspartate. This, relatively free, negative charge on aspartate can interact with positively-charged protons and facilitate their transport, thus increasing proton transport rate [The close proximity of fatty acid carboxylate group with aspartate results in increasing its pK_a and facilitates its binding to protons at pH 7.4 (the physiological pH) (27)]. On the other hand, based on the conformational analysis (Figure 4) and energy minimization modeling (Figure S17), it seems that none of the three single mutations has a substantial effect on the packing density of the transmembrane helices. Furthermore, elimination of one positive charge in single mutations does not have a significant effect on the overall positive charge on the matrix side of the protein. Finally, the disruption of the salt-bridge in single mutants does not seem to affect the synchronized interaction of odd numbered helices. It is worth mentioning that these structural analyses were based on the only available high-resolution structure of UCP2, which is locked in the cytoplasmic state and is in the zwitterionic detergent dodecylphosphocholine (36).

The proton transport rate in the double mutant protein is comparable to UCP2 (Figure 3a and Table 1). Regarding the increase in proton transport rates in the single mutants, this may seem counterintuitive; however, by considering a balance between the electrostatic and geometric factors influencing proton transport this observation can be explained. Disruption of two salt-bridges in the double mutant drastically influences the electric field of the original salt-bridge network and introduces two relatively free aspartate negative

charges that can interact with and attract protons, causing an increase in the proton transport rate. On the other hand, the distortion of the matrix salt-bridge network can influence the local conformation of the protein's interior, resulting in a tighter geometry of packing of transmembrane helices compared to the single mutants, thus limiting the accessibility of protons to the matrix (Figure S17). Furthermore, disruption of two salt-bridges may also prevent the synchronized interaction of the helices, thus interfering in the alternating conformational changes from matrix state to cytoplasmic state.

Reduced inhibition of ATP-related proton transport in mutants K141Q and K239Q is observable in Figure 3b, which suggests that the two residues might interact with ATP. These interactions could be interrupted in the two mutants either directly (via disruption of electrostatic interactions between lysine and phosphate groups of ATP) or indirectly (via conformational distortion of the binding site of ATP). Mutation of lysine 141 to glutamine is likely to disrupt the electrostatic interaction between lysine and the negatively-charged phosphate on the nucleotide (21). Using GDP as an inhibitor, NMR studies have indicated that the nucleotide binding site of UCP2 is close to transmembrane helices 1 to 4 (21). Interactions between lysine 141, arginine 185, and arginine 88 with GDP were previously proposed to have significant roles in holding GDP inside the protein's cavity (2,21). However, a series of systematic mutations on the ATP interacting residues are required to gain a better understanding of the interactions involved in the nucleotide-binding site of UCP2.

Self-association of UCP2 in lipid vesicles in comparison with AAC1

Self-association of members of the MCF family have been observed in several studies (41,42). Association of UCPs have also been reported previously (19,43); a group of researchers have suggested that UCPs form homodimers via establishing intermolecular disulfide bonds between the monomers (19). Homo- and hetero-multimer formation of UCP2 and UCP3 has also been proposed to be important for their function as mitochondrial calcium uniporters for calcium uptake in HeLa cells (44); addition of a mutated version of UCP2 interfered the calcium sequestration function of UCP3, while overexpression of either UCP2 or UCP3 alone could result in calcium uptake (44).

In the current and previous studies (3), we demonstrated that the dominant molecular form of UCP2 in PC vesicles is tetrameric (Figures 5 and 6). Tetrameric UCP2 and its mutants were all capable of transporting protons in the presence of long-chain fatty acids (such as PA) (3). Both UCP2 monomers and mixed multimers (comprised of monomeric, dimeric and tetrameric forms) in OG detergent associated to form a single tetrameric species in lipid vesicles. The hypothesis of tetramerization of UCP2 (as well as UCPs 1 (26), 4 and 5 (3)) has been supported previously by spectroscopic conformational analysis, using SDS (an anionic detergent denaturant) titration of the associated proteins (as proteoliposomes), as well as ultracentrifugation and mass spectrometric measurements (3). Titration of tetrameric UCP complexes resulted in the formation of dimers at low SDS concentrations (slightly above the detergent's CMC, $\gtrsim$ 2mM) and monomers at high SDS concentrations ($\gtrsim$ 83mM) (3). Gradual addition of SDS to proteoliposomes resulted in "stepwise" dissociation of human neuronal UCPs from tetramers to dimers, and from dimers to monomers (3). The observed molecular transition, further supported by the results of the current study (Figures 2, 5, and 6), is solely related to protein multimers dissociating to their constituents, and indicate that the higher order multimers (dimeric and tetrameric forms) are not artifacts of lipid and detergent complexes with the monomeric form of the protein and/or indefinite aggregation of UCPs in detergent, as has been suggested elsewhere (45, 46). Otherwise, intermediate bands (between 132, 66, and 33 kDa) should have been observed in SDS-PAGE as a consequence of gradual separation of these reagents from the monomeric protein. Spontaneous tetramerization of UCP2 (as well as UCP1) in the liposomes in the absence of detergents rules out the assumption of the existence of unidentified aggregated forms of the proteins as artifacts. The absence of a tetramer (~132 kDa) in the SDS-PAGE analysis of AAC1 proteoliposomes (Figure 6) and its different conformation from UCP2 (CD spectra in Figure 6) not only refutes the weakly-supported assumption of complex formation of MCF monomers with lipids and detergents (18), but also supports the idea of self-

association of UCP2 to its tetrameric form as a possible functional state. In fact, our results demonstrate that not all members of the MCF superfamily act in the same way in lipidic environments and the acquired molecular state is an inherent characteristic of the protein rather than a result of the experimental/environmental conditions. The overall pattern of the CD spectra (Figure 6) related to the tetrameric form of UCP2 is in good agreement with our previously reported studies on the molecular forms of reconstituted UCPs in similar types of liposomes (3,26).

The hypothesis that one of the functional forms of UCPs can be tetrameric (3) in a lipid environment is further supported by the MD simulations. The MD simulation results suggest that UCP2 is stable in a lipid bilayer and can potentially co-exist in monomeric and tetrameric forms. However, compared to the monomeric (and dimeric) UCP2, the tetramer is structurally more stabilized in the bilayer. This is mainly due to hydrophobic interactions as well as several hydrogen bonds and salt-bridges that form between the units (Figures S7-S9). In addition to the support coming from the structural features and interactions, the smaller SASA of the tetrameric UCP2 compared to the other forms suggest that the tetramer can be one of the functional forms of the protein in the membrane. Finally, the asymmetric characteristic of the tetramer suggests that all four of the UCP2 units may not be (simultaneously) functional.

Two possible interactions can contribute to oligomerization of UCP2: (i) protein-protein interactions; and (ii) protein-lipid-protein interactions, in which lipid molecules can facilitate the association of proteins. It was suggested that the presence of GXXXG motif in the sequence of transmembrane helices can promote the association of helices and increase inter-helical affinity (47). Association of helices inside the membrane has a vital role in oligomerization of membrane proteins (47) and in minimizing the free energy of insertion of polar residues into the membrane (48). UCP2 contains one GXXXG motif (GESQG) on one of the matrix side loops and three GXXXG motifs (GLVAG, GSTTG and GLWKG) on transmembrane helices 2, 3, and 4, respectively, all facing the same side of the protein (Figure S18) (40). The presence of three helix association promoters on the same side of UCP2 (also found in UCPs 1 and 3) could support the role of protein-protein interactions in self-association of the monomers to form dimers, which in turn might lead to the formation of tetramers (dimer of dimers). Only two of the three GXXXG motifs are present in UCPs 4, 5, and AAC1 (bovine and *Saccharomyces cerevisiae*) (23). Furthermore, our previous studies show that the presence of cardiolipin enhances self-association of UCP1 (26), which in turn enhances the impact of protein-lipid-protein interactions in oligomerization of UCPs. Overall, the current study strongly supports our proposed hypothesis on self-association of UCPs in lipid environments. Nevertheless, these findings are not in contradiction with the presence of monomers in the bilayer; indeed, both forms (as well as dimeric forms) might co-exist and be functional; or based on the physiological conditions and membrane's lipid composition, some multimeric states might be preferred over others in different cells.

Conclusions

This study is focused on the structure and proton transport function of UCP2 in lipidic environments. It has been proposed previously that the matrix salt-bridge network of MCF (49) and its positively charged amino acids in UCP2 might play important roles in substrate transport activity of the protein (23). We examined the role of the matrix-facing network in proton transport function of UCP2 by mutating positively charged amino acids (one/two at a time) to affect the salt-bridges. Based on the results of this study, the matrix network may have a filtering role on the proton transport function of UCP2; losing one salt-bridge in the network will result in an increase in the proton transport rate of the protein (twice more or higher). To explore the functional quaternary structure of UCP2, both pure monomeric forms as well as a mixture of monomeric, dimeric and tetrameric forms were reconstituted in lipid vesicles. Interestingly, both pure monomeric and the mixture of forms of UCP2 were spontaneously transformed to tetrameric forms after reconstitution in lipid vesicles. AAC1, a structurally comparable protein to UCPs, and a member of MCF, did not show tetrameric forms after reconstitution in lipid bilayers.

The stability of tetrameric UCP2 was further confirmed by MD simulations. Compared to

its monomeric form, the tetrameric UCP2 showed enhanced helicity and stability during the simulation. The MD results also indicated that both monomeric and tetrameric forms were structurally more stable than the dimeric forms, while average SASA suggested that the tetrameric UCP2 in lipid environments was more stable than the monomeric protein. Overall, these findings showed that not all members of MCF adopt the same monomeric/multimeric state in lipidic environments. Furthermore, contrary to what have been reported previously (45), monomeric form is not the only functional form of UCPs.

Experimental Procedures

Chemicals

L-α-Phosphatidylcholine type X-E (L-α-PC) was from Sigma (St. Louis, Missouri). This lipid was extracted from dry egg yolk and contained more than 60% (by weight) phosphatidylcholine; the remaining lipids were mostly phosphatidylethanolamine and other phospholipids. C_8E_4 was from Bachem (Bubendorf, Switzerland). Octylglucopyranoside (OG) was obtained from BioVision (San Francisco, California). SPQ [6-methoxy-N-(3- sulfopropyl) quinolinium; 99% purity] was from Biotium (Fremont, California). Other chemicals were from Sigma.

Site-directed mutagenesis and transformation

Four cDNAs (complementary DNA), encoding three single mutant and one double mutant version of UCP2 were generated by site-directed mutagenesis. The mutated cDNAs were used to encode proteins with either single (K38Q, K239Q and K141Q) or double (K38Q/K239Q) point mutations at their matrix side salt-bridge network (Figure 1 and S1). Overlap extension PCR (polymerase chain reaction) was used to incorporate the mutations into cDNAs (50). The Wild-type N-terminally His (histidine)-tagged human UCP2 in pET26b(+) vector was employed as a template to create two fragments of cDNA with overlapping ends (3). The two fragments of cDNA were generated by flanking and mutagenic primers (primer A+ mutagenic primer B for generating the first PCR product and mutagenic primer C+ flanking primer D for generating the second PCR product). The PCR products were isolated and hybridized through a third PCR reaction in the presence of flanking primers A and D to generate the mutant cDNAs. In the case of the double mutant, the single mutant cDNA was used as the template for an extra overlap extension PCR which introduced the second point mutation into the cDNA. The mutant cDNAs were then digested with appropriate restriction enzymes (NcoI-HF and HindIII-HF), ligated into pET26b(+) vector and transformed into competent DH5α *E. coli* cells by heat-shock. The identity of mutants was confirmed by DNA sequencing (TCAG, Center for Applied Genomics, Toronto, ON, Canada). The recombinant vectors encoding wild-type and mutant versions of UCP2 were transformed into BL21-Codon Plus- RIPL *E. coli* (*E. coli* BL21 CD+) cells by heat shock. In the case of AAC1, codon-optimized recombinant N-terminally His-tagged bovine AAC1 in pET26b(+) was transformed into BL21 *E. coli* cells using the same methodology.

Overexpression and membrane extraction of proteins

Recombinant versions of UCP2, the mutants and AAC1 were expressed in *E. coli* BL21(or BL21 CD+) cells using the auto-induction method as previously described for UCP1 (25,26). Briefly, the bacterial cells were incubated for 22 hours in the auto-induction media [0.5% yeast extract, 0.5% glycerol, 1% tryptone, 0.2% lactose, 0.05% glucose, 50 mM KH_2PO_4, 50mM Na_2HPO_4, 1mM $MgSO_4$, 25 mM $(NH_4)_2SO_4$] at 22 °C. After 22 hours the media were centrifuged at 8000 *g* for 15 minutes and the bacterial cells (pellets) were collected. The pellets were resuspended in lysis buffer [500 mM NaCl and 20 mM Tris-HCl pH 8.0, one EDTA (ethylenediaminetetraacetic acid)-free complete protease inhibitor tablet (Basel, Switzerland), 0.5 mg/ml DNase and 0.2 mg/ml lysozyme]. A high-pressure cell disruptor (Constant Systems Limited, Daventry, UK) was used to lyse the cells (at 20 kPsi). The lysate was centrifuged for 20 minutes at 20000 *g* to remove intact cells or aggregated proteins. The supernatant was collected and ultracentrifuged at 50000 *g* (MLA 80 rotor, Beckman Coulter) for 1 hour to obtain the bacterial membranes in the pellet.

Purification of proteins using immobilized metal affinity chromatography

Binding buffer containing 20 mM Tris-HCl, 1 mM THP [Tris (hydroxypropyl) phosphine], 500 mM NaCl, 1% LDAO (lauryldimethylamine oxide) detergent and 10 mM imidazole was used to solubilize the bacterial membrane. The solution was then incubated with Ni-NTA (Nickel-nitrilotriacetic acid, Thermo Scientific Waltham, Massachusetts) resin for 2 hours and subsequently transferred to a column. In the case of UCP2 and its mutants the resin in the column was washed with 12 mM imidazole, and successively eluted with 25, 40 and 400 mM of imidazole in 1% OG (octyl-beta-glucoside) detergent. The mixture of monomer and associated molecular forms of proteins were eluted at 40 mM imidazole (Figure 2a), and the pure monomer was eluted at 25 mM of imidazole. For AAC1, the column was washed with 30 mM imidazole and eluted with 400 mM imidazole in 1% OG detergent. Econo-Pac 10DG Columns (Bio-Rad, Hercules, California) were used to desalt the fractions. The purity and concentration of proteins were analyzed with SDS-PAGE (sodium dodecyl sulfate–polyacrylamide gel electrophoresis) and modified Lowry assay, respectively (51). The desalted proteins were kept in desalting buffer (20 mM Tris-HCl, 1% OG, 1% glycerol, pH 8.0) and stored at -80° C.

Western blot analysis

The identity of overexpressed recombinant wild-type UCP2, its mutants, and AAC1 were confirmed by immunoblotting. Proteins (5-10 µg) were loaded on SDS-PAGE gels, and using the semi-dry technique, the proteins were transferred (75 minutes -110 volts) to nitrocellulose. The filters were stained with Amido Black to confirm transfer efficiency. The nitrocellulose filters were blocked for at least 60 minutes in Tris buffered saline containing 0.1% tween-20 and 5% dry skim milk. The primary antibody used to detect UCP2 and its mutants was 1:2000 dilution of anti-UCP1/2/3 raised in rabbit (Santa Cruz Biotechnology Inc. Dallas, Texas), and for AAC1 the primary antibody was 1:5000 dilution of rabbit IgG anti-AAC1 (Bio-Rad). The secondary antibody was 1:5000 dilution of horseradish peroxidase (HRP) conjugated antibody raised against rabbit (Rockland, Limerick, Pennsylvania). Luminata Crescendo western HRP substrate (Millipore Sigma) was used as a chemiluminescent reagent to achieve immunodetection. A Bio-Rad VersaDoc imaging system was employed to capture the image.

Reconstitution in lipid vesicles

Reconstitution of UCP2, the mutants and AAC1 into lipid vesicles followed the procedure as described previously (3,24), with minor modifications. Briefly, solutions of egg yolk PC in MeOH: Chloroform (1:3) were dried for 8-12 hours under vacuum. The dried lipids were solubilized in appropriate reconstitution buffer (supplemented with 3mM SPQ (6-methoxy-1-(3-sulfonatopropyl) quinolinium) fluorescent probe in proton transport assays) to generate multilamellar vesicles. The multilamellar vesicles were solubilized in C_8E_4 detergent to form lipid-detergent mixed micelles [at a lipid/detergent ratio of 1/2.5 (w/w)]. Pure proteins were added to the mixed micelles to a final 3 µM concentration. Protein/lipid ratio was ~1/6000 (mol/mol) for proton transport and ~1/600 (mol/mol) for CD (circular dichroism) experiments. Unilamellar proteoliposomes were spontaneously generated by removing the detergent using SM-2 Biobeads (Bio-Rad). The average radii of the prepared proteoliposomes for the proton transport assays and CD measurements were 76.87±2.29 nm and 31.46±1.68 nm, respectively, as determined by dynamic light scattering. On average, the radii of the blank liposomes were ~13% larger than the proteoliposomes in both cases. In proton transport assays, part of the added SPQ was entrapped inside the liposomes and the external SPQ was removed by size-exclusion chromatography, using a Sephadex G25-300 (GE-Healthcare, Chicago, Illinois) spin column. Blank (protein-free) liposomes were prepared in parallel with proteoliposomes.

CD spectroscopy and fluorescence measurements

Far-UV CD measurements were performed at 25 °C, and at 1 nm resolution on an AVIV 215 spectropolarimeter (Aviv Biomedical, Lakewood, New Jersey). Quartz cells with 0.1 cm path length were used for measuring the CD spectra of the proteins in OG detergent and in liposomes. Ellipticities were converted to mean residue ellipticity, [θ]. Each spectrum was an average of 6-12 measurements.

Steady-state fluorescence of the liposomes was performed using a Cary Eclipse spectrophotometer (Varian, Palo Alto, California) with a band width slit of 5 nm and a scan speed of 600 nm/min. Excitation and emission of the SPQ fluorescence signal were at 347 and 442 nm, respectively. The fluorescence scans were performed at 25 °C. Each proton transport analysis was an average of 10 different scans.

Proton transport measurements

Proton transport rates of the proteins were measured following their reconstitution in lipid vesicles, as described previously (24). Anions quench SPQ by a dynamic collision mechanism. In proton transport assays, 40 µL of liposomes were mixed with 1.96 mL of external buffer. The internal buffer was composed of TEA_2SO_4 (TEA: tetraethylammonium, 54 mM), TES buffer (20 mM) and EDTA (0.7 mM). The external buffer had a similar composition to the internal buffer, with TEA_2SO_4 replaced by K_2SO_4 (54 mM). The pH of both buffers was kept constant at 7.2. Palmitic acid (PA, final concentration 100 µM) was used to activate UCP2-mediated proton flux. Addition of valinomycin mediated the influx of K^+ which triggered fatty acid dependent proton efflux of UCP2 (and its mutants). Proton efflux by UCP2 (and the mutants) resulted in deprotonation of TES buffer. TES^- anions quenched the SPQ emission. The rate of the decrease in SPQ fluorescence signal was correlated to the rate of fatty acid activated proton transport of UCP2 and its mutants. The rate of fatty acid activated proton transport was measured by monitoring the decrease in SPQ's fluorescence signal intensity within the first 30 seconds after addition of valinomycin (26). All proton transport data in liposomes were corrected for the basal non-specific leakage by subtraction of blank liposomes proton efflux. Furthermore, the proton transport data were calibrated for internal volume, SPQ's fluorescence response and protein concentration. The concentration of proteins in proteoliposomes was calculated using a modified Lowry assay (24,51).

Structural modeling of UCP2 and mutants

The structure of UCP2 (PDB ID: 2LCK) was viewed and analyzed with UCSF Chimera 1.13 (40). Chimera 1.13 was also used to generate mutants, to find the lowest energy conformations and to analyze the structural changes occurred by mutations.

Statistical analysis

One-way analysis of variance (ANOVA) was used as the statistical method to analyze the data. $P<0.05$ was considered as statistically significant.

MD simulations

The only available high-resolution NMR structure of UCP2 (PDB ID: 2LCK) (21) was used as the starting structure of the monomeric UCP2. The same structure was used to build the dimeric and tetrameric forms. To form the multimeric UCP2, the monomer units were aligned in such a way that the transmembrane helices 2, 3, and 4 that contain GXXXG motifs, be involved in the interactions with the neighboring unit(s) (Figure S18); GXXXG motifs have been proposed to play a role in the oligomerization of UCP2 (47). Figure S19 shows the initial and final structures of the multimeric forms with respect to the GXXXG motif. Moreover, in the case of dimer, several relative orientations for the monomers were examined, among which the one with maximal (distance-based) favorable interactions (electrostatic and hydrophobic) was chosen for the simulations. Similarly, the tetramer was built from two dimers allowing for maximal favorable interactions.

The protein-membrane systems were built using the CHARMM-GUI online server (52). Membranes were built with 300, 316, and 498 1-palmitoyl-2-oleoylphosphatidylcholine (POPC) units for the monomeric, dimeric, and tetrameric UCP2, respectively. Each system was solvated in an explicit TIP3P (53) box (total of 24195, 28463, and 47881 water molecules for monomer, dimer, and tetramer, respectively) and neutralized with 0.15 M KCl (65, 78, and 134 K^+, and 80, 108, and 194 Cl^- for the monomer, dimer, and tetramer, respectively) to ensure charge neutrality. CHARMM36m/CHARMM36 protein/lipid forcefield were used (54,55). All systems were first minimized using steepest descents algorithm followed by 375 ps of equilibration under constant volume and temperature (NVT), and constant pressure and temperature (NPT) conditions. Molecular Dynamics (MD) simulations were

conducted for 150 ns with 2 ps timesteps using GROMACS/2018 (56). Chemical bonds were constrained using the linear constraint solver (P-LINCS) algorithm (57). The Nosé-Hoover thermostat (58,59) was employed to maintain the temperature at 300 K with a 1.0 ps coupling constant and the Parrinello–Rahman barostat (60) with a compressibility of 4.5×10^{-5} bar^{-1} and a 5 ps coupling constant was used. The particle mesh Ewald method (61,62) was used for the long-range interactions. The above protocol and methods have been shown to be reliable in a number of previous studies (*e.g.*, Refs. (63-65) and references therein).

Acknowledgements

This work was supported by grants from the Canada Foundation for Innovation (CFI) to MJN and MDS and the Natural Sciences and Engineering Research Council of Canada (NSERC) to MJN, MDS and MK and NSERC and Canada Research Chairs Program (CRC) to MK. Computational resources were provided by Compute Canada. AA is the recipient of an Ontario Trillium Scholarship (OTS).

Conflict of Interest

The authors declare that they have no conflicts of interest with the contents of this article.

References

1. Krauss, S., Zhang, C.-Y., and Lowell, B. B. (2005) The mitochondrial uncoupling-protein homologues. *Nat. Rev. Mol. Cell Biol.* **6**, 248-261
2. Jezek, P., Holendova, B., Garlid, K. D., and Jaburek, M. (2018) Mitochondrial Uncoupling Proteins: Subtle Regulators of Cellular Redox Signaling. *Antioxid. Redox Signal.* **29**, 667-714
3. Hoang, T., Kuljanin, M., Smith, M. D., and Jelokhani-Niaraki, M. (2015) A biophysical study on molecular physiology of the uncoupling proteins of the central nervous system. *Biosci. Rep*. **35,** e00226
4. Andrews, Z. B., Diano, S., and Horvath, T. L. (2005) Mitochondrial uncoupling proteins in the CNS: in support of function and survival. *Nat. Rev. Neurosci*. **6**, 829
5. Zackova, M., Skobisova, E., Urbankova, E., and Jezek, P. (2003) Activating omega-6 polyunsaturated fatty acids and inhibitory purine nucleotides are high affinity ligands for novel mitochondrial uncoupling proteins UCP2 and UCP3. *J. Biol. Chem.* **278**, 20761-20769
6. Donadelli, M., Dando, I., Fiorini, C., and Palmieri, M. (2014) UCP2, a mitochondrial protein regulated at multiple levels. *Cell Mol. Life Sci.* **71**, 1171-1190
7. Echtay, K. S., Roussel, D., St-Pierre, J., Jekabsons, M. B., Cadenas, S., Stuart, J. A., Harper, J. A., Roebuck, S. J., Morrison, A., and Pickering, S. (2002) Superoxide activates mitochondrial uncoupling proteins. *Nature* **415**, 96
8. Brand, M. D., Affourtit, C., Esteves, T. C., Green, K., Lambert, A. J., Miwa, S., Pakay, J. L., and Parker, N. (2004) Mitochondrial superoxide: production, biological effects, and activation of uncoupling proteins. *Free Radic. Biol. Med*. **37**, 755-767
9. Li, N., Karaca, M., and Maechler, P. (2017) Upregulation of UCP2 in beta-cells confers partial protection against both oxidative stress and glucotoxicity. *Redox Biol.* **13**, 541-549
10. Lytovchenko, O., and Kunji, E. R. S. (2017) Expression and putative role of mitochondrial transport proteins in cancer. *Biochim. Biophys. Acta* **1858**, 641-654
11. Ayyasamy, V., Owens, K. M., Desouki, M. M., Liang, P., Bakin, A., Thangaraj, K., Buchsbaum, D. J., LoBuglio, A. F., and Singh, K. K. (2011) Cellular model of Warburg effect identifies tumor promoting function of UCP2 in breast cancer and its suppression by genipin. *PLoS One* **6**, e24792
12. Li, W., Nichols, K., Nathan, C.-A., and Zhao, Y. (2013) Mitochondrial uncoupling protein 2 is up-regulated in human head and neck, skin, pancreatic, and prostate tumors. *Cancer Biomarkers* **13**, 377-383
13. Kuai, X.-Y., Ji, Z.-Y., and Zhang, H.-J. (2010) Mitochondrial uncoupling protein 2 expression in colon cancer and its clinical significance. *World J. Gastroenterol: WJG* **16**, 5773
14. Deng, S., Yang, Y., Han, Y., Li, X., Wang, X., Zhang, Z., and Wang, Y. (2012) UCP2 inhibits ROS-mediated apoptosis in A549 under hypoxic conditions. *PLoS One* **7**, e30714
15. Ježek, P., Engstová, H., Žáčková, M., Vercesi, A. E., Costa, A. D., Arruda, P., and Garlid, K. D. (1998) Fatty acid cycling mechanism and mitochondrial uncoupling proteins. *Biochim. Biophys. Acta (BBA)-Bioenergetics* **1365**, 319-327
16. Winkler, E., and Klingenberg, M. (1994) Effect of fatty acids on H+ transport activity of the reconstituted uncoupling protein. *J. Biol. Chem.* **269**, 2508-2515
17. Fedorenko, A., Lishko, P. V., and Kirichok, Y. (2012) Mechanism of fatty-acid-dependent UCP1 uncoupling in brown fat mitochondria. *Cell* **151**, 400-413
18. Crichton, P. G., Harding, M., Ruprecht, J. J., Lee, Y., and Kunji, E. R. (2013) Lipid, detergent, and Coomassie Blue G-250 affect the migration of small membrane proteins in blue native gels: mitochondrial carriers migrate as monomers not dimers. *J. Biol. Chem*. **288**, 22163-22173
19. Klingenberg, M., and Appel, M. (1989) The uncoupling protein dimer can form a disulfide cross-link between the mobile C-terminal SH groups. *FEBS J.* **180**, 123-131
20. Pebay-Peyroula, E., Dahout-Gonzalez, C., Kahn, R., and Trézéguet, V. (2003) Structure of mitochondrial ADP/ATP carrier in complex with carboxyatractyloside. *Nature* **426**, 39

21. Berardi, M. J., Shih, W. M., Harrison, S. C., and Chou, J. J. (2011) Mitochondrial uncoupling protein 2 structure determined by NMR molecular fragment searching. *Nature* **476**, 109-113
22. Robinson, A. J., Overy, C., and Kunji, E. R. (2008) The mechanism of transport by mitochondrial carriers based on analysis of symmetry. *Proc. Natl. Acad. Sci. U S A* **105**, 17766-17771
23. Hoang, T., Matovic, T., Parker, J., Smith, M. D., and Jelokhani-Niaraki, M. (2015) Role of positively charged residues of the second transmembrane domain in the ion transport activity and conformation of human uncoupling protein-2. *Biochemistry* **54**, 2303-2313
24. Hoang, T., Smith, M. D., and Jelokhani-Niaraki, M. (2012) Toward understanding the mechanism of ion transport activity of neuronal uncoupling proteins UCP2, UCP4, and UCP5. *Biochemistry* **51**, 4004-4014
25. Studier, F. W. (2005) Protein production by auto-induction in high-density shaking cultures. *Protein expr. purif.* **41**, 207-234
26. Hoang, T., Smith, M. D., and Jelokhani-Niaraki, M. (2013) Expression, folding, and proton transport activity of human uncoupling protein-1 (UCP1) in lipid membranes: evidence for associated functional forms. *J. Biol. Chem.* **288**, 36244-36258
27. Bertholet, A. M., and Kirichok, Y. (2017) UCP1: A transporter for H(+) and fatty acid anions. *Biochimie* **134**, 28-34
28. Klingenberg, M. (2010) Wanderings in bioenergetics and biomembranes. *Biochim. Biophys. Acta* **1797**, 579-594
29. Jabůrek, M., Vařecha, M., Gimeno, R. E., Dembski, M., Ježek, P., Zhang, M., Burn, P., Tartaglia, L. A., and Garlid, K. D. (1999) Transport function and regulation of mitochondrial uncoupling proteins 2 and 3. *J. Biol. Chem.* **274**, 26003-26007
30. Klingenberg, M., and Echtay, K. S. (2001) Uncoupling proteins: the issues from a biochemist point of view. *Biochim. Biophys. Acta (BBA)-Bioenergetics* **1504**, 128-143
31. Greenfield, N. J., and Fasman, G. D. (1969) Computed circular dichroism spectra for the evaluation of protein conformation. *Biochemistry* **8**, 4108-4116
32. Toniolo, C., Polese, A., Formaggio, F., Crisma, M., and Kamphuis, J. (1996) Circular dichroism spectrum of a peptide 310-helix. *J. Am. Chem. Soc.* **118**, 2744-2745
33. Cooper, T. M., and Woody, R. W. (1990) The effect of conformation on the CD of interacting helices: a theoretical study of tropomyosin. *Biopolymers* **30**, 657-676
34. Salom, D., Hill, B. R., Lear, J. D., and DeGrado, W. F. (2000) pH-dependent tetramerization and amantadine binding of the transmembrane helix of M2 from the influenza A virus. *Biochemistry* **39**, 14160-14170
35. Sala, F. A., Valadares, N. F., Macedo, J. N., Borges, J. C., and Garratt, R. C. (2016) Heterotypic coiled-coil formation is essential for the correct assembly of the septin heterofilament. *Biophys. J.* **111**, 2608-2619
36. Zoonens, M., Comer, J., Masscheleyn, S., Pebay-Peyroula, E., Chipot, C., Miroux, B., and Dehez, F. (2013) Dangerous liaisons between detergents and membrane proteins. The case of mitochondrial uncoupling protein 2. *J. Am. Chem. Soc.* **135**, 15174-15182
37. Bond, P. J., and Sansom, M. S. (2003) Membrane protein dynamics versus environment: simulations of OmpA in a micelle and in a bilayer. *J. Mol. Biol.* **329**, 1035-1053
38. Yaacob, N., Ahmad Kamarudin, N. H., Leow, A. T. C., Salleh, A. B., Raja Abd Rahman, R. N. Z., and Mohamad Ali, M. S. (2017) The Role of Solvent-Accessible Leu-208 of Cold-Active Pseudomonas fluorescens Strain AMS8 Lipase in Interfacial Activation, Substrate Accessibility and Low-Molecular Weight Esterification in the Presence of Toluene. *Molecules* **22**, 1312
39. Lopes-Rodrigues, M., Triguero, J., Torras, J., Perpète, E. A., Michaux, C., Zanuy, D., and Alemán, C. (2018) Influence of the surrounding environment in re-naturalized β-barrel membrane proteins. *Biophys. Chem.* **234**, 6-15
40. Pettersen, E. F., Goddard, T. D., Huang, C. C., Couch, G. S., Greenblatt, D. M., Meng, E. C., and Ferrin, T. E. (2004) UCSF Chimera—a visualization system for exploratory research and analysis. *J. Comput. Chem.* **25**, 1605-1612

41. Schroers, A., Burkovski, A., Wohlrab, H., and Krämer, R. (1998) The Phosphate Carrier from Yeast Mitochondria DIMERIZATION IS A PREREQUISITE FOR FUNCTION. *J. Biol. Chem.* **273**, 14269-14276
42. Kotaria, R., Mayor, J. A., Walters, D. E., and Kaplan, R. S. (1999) Oligomeric state of wild-type and cysteine-less yeast mitochondrial citrate transport proteins. *J. Bioenerg. Biomembr.* **31**, 543-549
43. Rebuffet, E., Frick, A., Jarva, M., and Tornroth-Horsefield, S. (2017) Cell-free production and characterisation of human uncoupling protein 1-3. *Biochem. Biophys. Rep.* **10**, 276-281
44. Trenker, M., Malli, R., Fertschai, I., Levak-Frank, S., and Graier, W. F. (2007) Uncoupling proteins 2 and 3 are fundamental for mitochondrial Ca2+ uniport. *Nat. Cell. Biol.* **9**, 445-452
45. Lee, Y., Willers, C., Kunji, E. R., and Crichton, P. G. (2015) Uncoupling protein 1 binds one nucleotide per monomer and is stabilized by tightly bound cardiolipin. *Proc. Natl. Acad. Sci. U S A* **112**, 6973-6978
46. Crichton, P. G., Lee, Y., and Kunji, E. R. (2017) The molecular features of uncoupling protein 1 support a conventional mitochondrial carrier-like mechanism. *Biochimie* **134**, 35-50
47. Russ, W. P., and Engelman, D. M. (2000) The GxxxG motif: A framework for transmembrane helix-helix association1. *J. Mol. Biol.* **296**, 911-919
48. Popot, J.-L., and Engelman, D. M. (1990) Membrane protein folding and oligomerization: the two-stage model. *Biochemistry* **29**, 4031-4037
49. Robinson, A. J., and Kunji, E. R. (2006) Mitochondrial carriers in the cytoplasmic state have a common substrate binding site. *Proc. Natl. Acad. Sci. U S A* **103**, 2617-2622
50. Heckman, K. L., and Pease, L. R. (2007) Gene splicing and mutagenesis by PCR-driven overlap extension. *Nat. Protoc.* **2**, 924
51. Peterson, G. L. (1977) A simplification of the protein assay method of Lowry et al. which is more generally applicable. *Anal. Biochem.* **83**, 346-356
52. Lee, J., Cheng, X., Swails, J. M., Yeom, M. S., Eastman, P. K., Lemkul, J. A., Wei, S., Buckner, J., Jeong, J. C., and Qi, Y. (2015) CHARMM-GUI input generator for NAMD, GROMACS, AMBER, OpenMM, and CHARMM/OpenMM simulations using the CHARMM36 additive force field. *J. Chem. Theory Comput.* **12**, 405-413
53. Jorgensen, W. L., Chandrasekhar, J., Madura, J. D., Impey, R. W., and Klein, M. L. (1983) Comparison of simple potential functions for simulating liquid water. *J. Chem. Phys.* **79**, 926-935
54. Huang, J., Rauscher, S., Nawrocki, G., Ran, T., Feig, M., de Groot, B. L., Grubmüller, H., and MacKerell Jr, A. D. (2016) CHARMM36m: an improved force field for folded and intrinsically disordered proteins. *Nat. Methods* **14**, 71
55. Lee, S., Tran, A., Allsopp, M., Lim, J. B., Hénin, J. R. M., and Klauda, J. B. (2014) CHARMM36 united atom chain model for lipids and surfactants. *J. Phys. Chem. B* **118**, 547-556
56. Abraham, M. J., Murtola, T., Schulz, R., Páll, S., Smith, J. C., Hess, B., and Lindahl, E. (2015) GROMACS: High performance molecular simulations through multi-level parallelism from laptops to supercomputers. *SoftwareX* **1**, 19-25
57. Hess, B. (2008) P-LINCS: A parallel linear constraint solver for molecular simulation. *J. Chem. Theory Comput.* **4**, 116-122
58. Nosé, S. (1984) A unified formulation of the constant temperature molecular dynamics methods. *J. Chem. Phys.* **81**, 511-519
59. Hoover, W. G. (1985) Canonical dynamics: equilibrium phase-space distributions. *Phys. rev. A* **31**, 1695
60. Parrinello, M., and Rahman, A. (1981) Polymorphic transitions in single crystals: A new molecular dynamics method. *J. Appl. Phys.* **52**, 7182-7190
61. Darden, T., York, D., and Pedersen, L. (1993) Particle mesh Ewald: An N· log (N) method for Ewald sums in large systems. *J. Chem. Phys.* **98**, 10089-10092
62. Essmann, U., Perera, L., Berkowitz, M. L., Darden, T., Lee, H., and Pedersen, L. G. (1995) A smooth particle mesh Ewald method. *J. Chem. Phys.* **103**, 8577-8593

63. Wong-ekkabut, J., and Karttunen, M. (2012) Assessment of common simulation protocols for simulations of nanopores, membrane proteins, and channels. *J. Chem. Theory Comput.* **8**, 2905-2911
64. Wong-ekkabut, J., and Karttunen, M. (2016) The good, the bad and the user in soft matter simulations. *Biochim. Biophys. Acta (BBA)-Biomembranes* **1858**, 2529-2538
65. Göddeke, H., Timachi, M. H., Hutter, C. A., Galazzo, L., Seeger, M. A., Karttunen, M., Bordignon, E., and Schäfer, L. V. (2018) Atomistic mechanism of large-scale conformational transition in a heterodimeric ABC exporter. *J. Am. Chem. Soc.* **140**, 4543-4551

Footnote

AAC1, mitochondrial ADP/ATP carrier protein; C_8E_4, tetraethylene glycol monooctyl ether; IMM, inner mitochondrial membrane; IMS, mitochondrial intermembrane space; LDAO, n-dodecyl-N,N-Dimethylamine-N-oxide; MCF, mitochondrial carrier superfamily; MD, molecular dynamics; OG, octylglucopyranoside; PA, phosphatidic acid; PC, phosphatidylcholine; PCA, principal component analysis, PelB, pectate lyase B; PI, Phosphatidylinositol; POPC, 1-palmitoyl-2-oleoylphosphatidylcholine; RMSD, root mean square deviation; RMSF, root mean square fluctuation; ROS, reactive oxygen species; SASA, solvent accessible surface area; SPQ, 6-methoxy-N-(3-sulfopropyl)quinolinium; TEA, tetraethylammonium; TES, N-[tris(hydroxymethyl)methyl]-2-aminoethane-sulfonic acid; UCP, uncoupling protein.

Table 1. Proton transport rate of UCP2 and its mutants in the absence and presence of 500 μM ATP. All the units are in μmol of proton/min/mg of protein

protein	proton transport rate (no ATP)	proton transport rate (500 μM ATP)
UCP2	2.43 ± 0.16	0.70 ± 0.03
K38Q	6.93 ± 0.25	3.06 ± 0.29
K141Q	5.74 ± 0.02	2.89 ± 0.39
K239Q	7.16 ± 0.23	1.47 ± 0.10
K38Q/K239Q	1.58 ± 0.04	0.70 ± 0.10

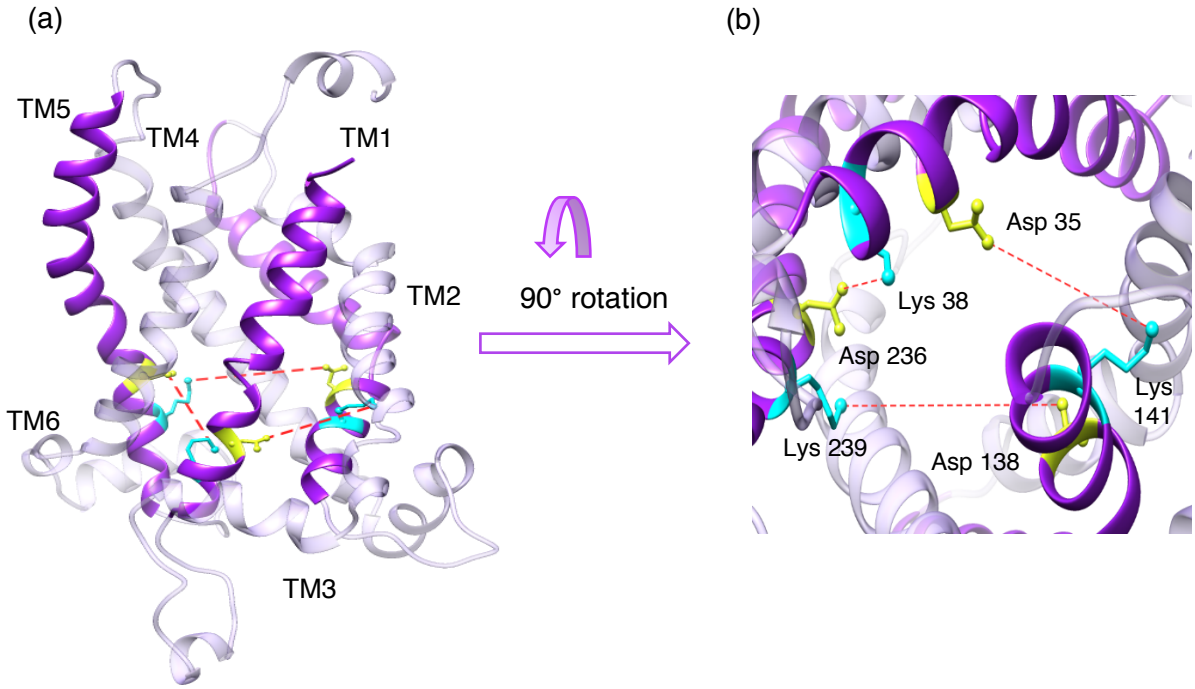

Figure 1. Lateral and matrix side top views of UCP2 (PDB ID: 2LCK) (a) Lateral view of UCP2; the matrix salt bridge network is represented with red dashed lines. Positively charged (lysine) and negatively charged (aspartate) amino acids in both networks are highlighted in cyan and yellow, respectively. Transmembrane domains are numbered as TM1 to TM6; TM1, TM3 and TM5 are shown in dark purple and TM2, TM4 and TM5 are shown in pale purple. **(b) The top view of the matrix-facing network** illustrates the salt-bridges involved. The residues involved in the network are shown with three letter codes and numbers.

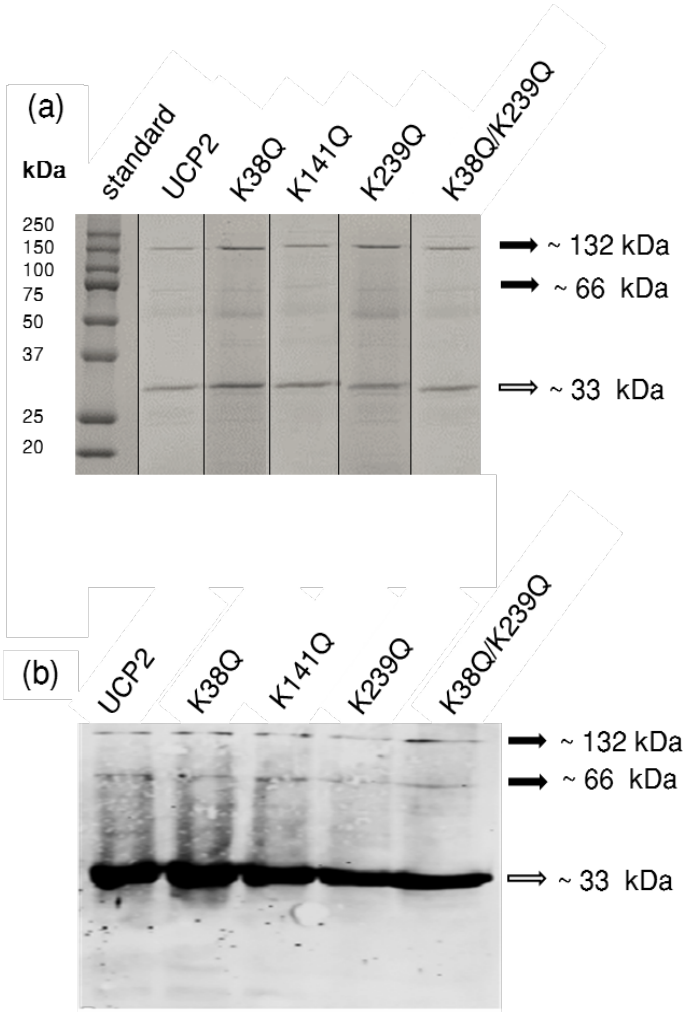

Figure 2. (a) Purified UCP2 and mutants in OG detergent, analyzed using SDS PAGE stained with coomassie blue. Solid arrows show the location of associated forms and open arrows show the location of monomers. Black vertical lines separate individual runs. **(b) Western blot analysis of UCP2 and its mutants in OG detergent probed with an α-UCP 1, 2, 3 antibody** confirms the presence of UCP2 in monomeric, dimeric and tetrameric forms.

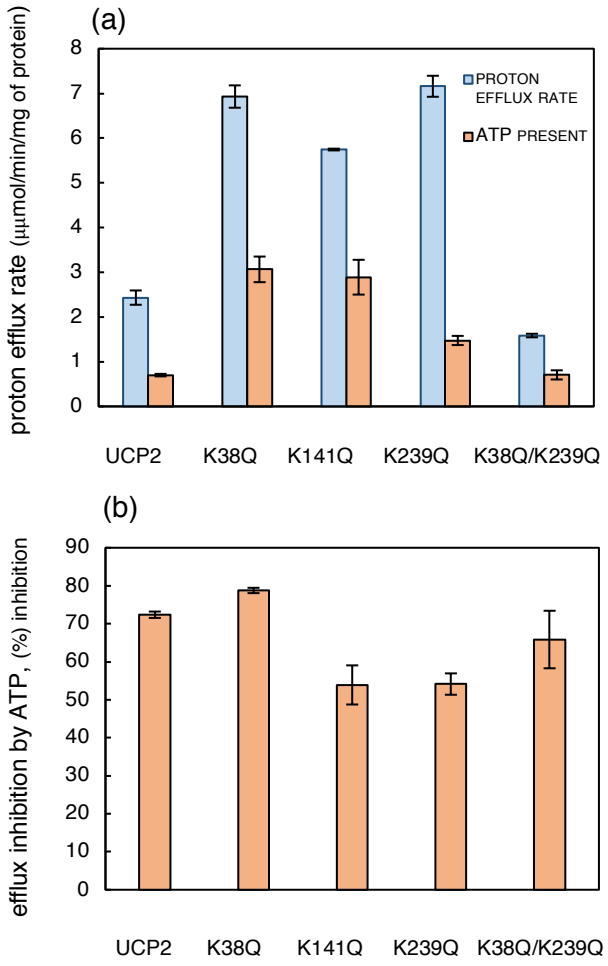

Figure 3. (a) Proton transport rate of UCP2 and its mutants. Each bar represents the average transport rate of 10 repeats and the error bars show the standard deviations. **(b) Percentage of proton efflux inhibition by ATP.**

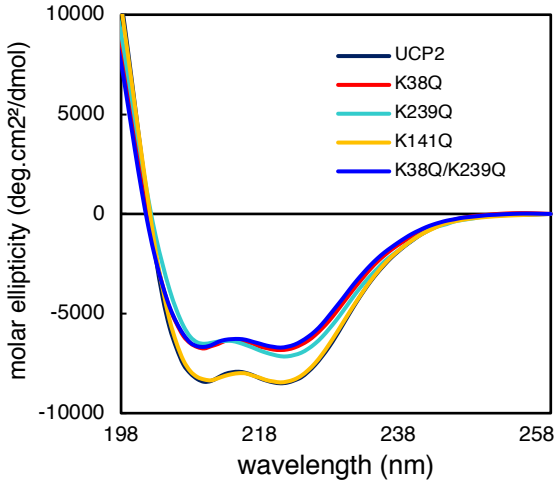

Figure 4. CD spectra of UCP2 and its mutants in OG detergent. The CD spectrum for each protein was the average of 6 scans. The overall conformation of UCP2 is not altered in mutants and all spectra show the characteristics of α-helical proteins. The concentrations of the analyzed proteins were between 5 to 8 μM.

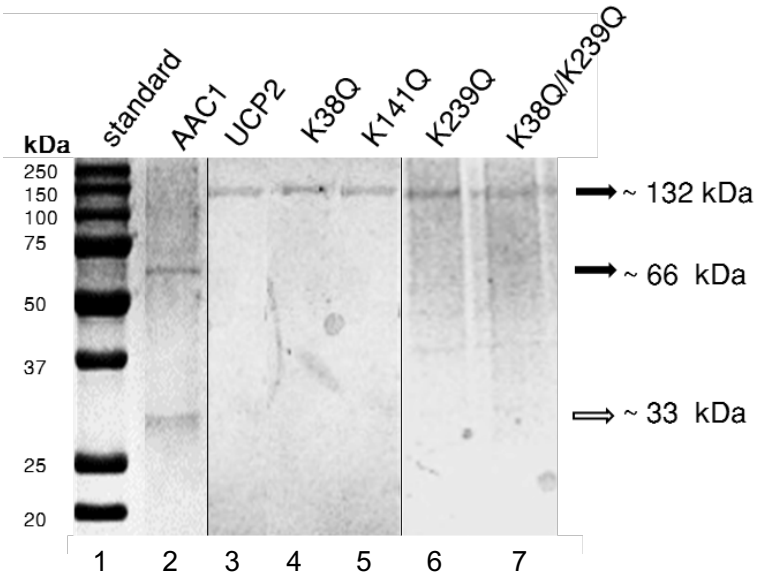

Figure 5. SDS-PAGE analysis of proteoliposomes shows the presence of the tetrameric form of UCP2 (and its mutants), and mixture of monomeric and dimeric forms of AAC1 in lipid vesicles. Black vertical lines separate individual gels.

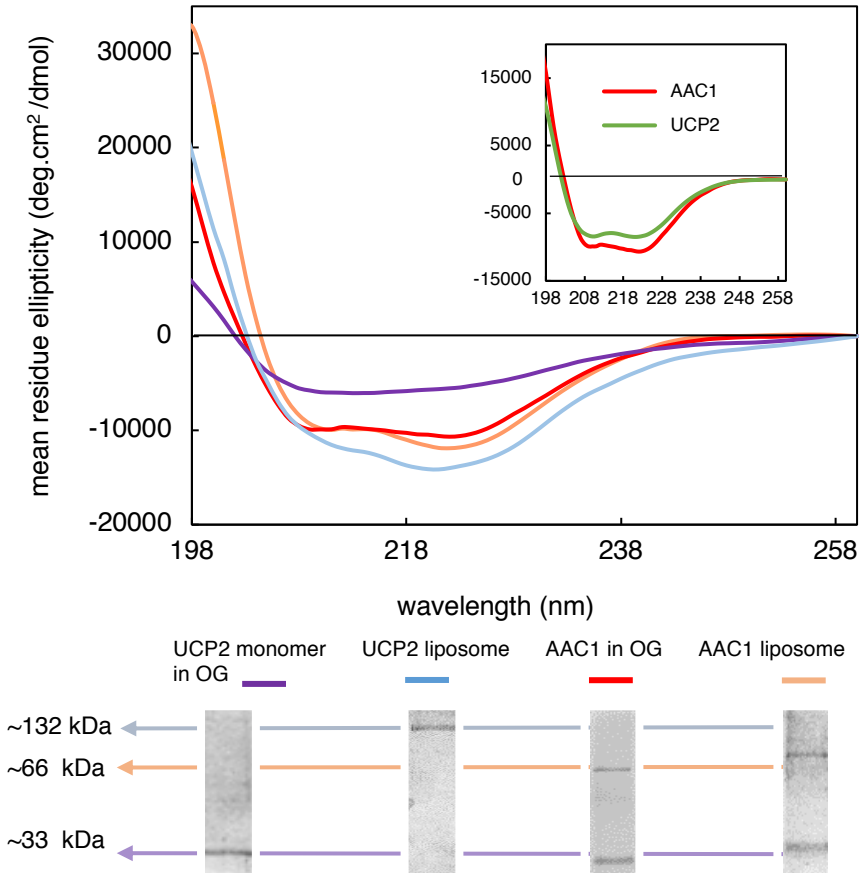

Figure 6. CD spectra and coomassie stained SDS-PAGE gel image of UCP2 and AAC1 before (in OG detergent) and after reconstitution in PC liposomes. Reconstitution of UCP2 monomer in PC vesicles resulted in formation of tetramers. AAC1 retained its mixed monomeric and dimeric states after reconstitution. The change in CD spectra of UCP2 confirms the alteration of its structure. The inset shows the comparable spectra of UCP2 (mixture of monomeric, dimeric and tetrameric forms) and AAC1 (mixture of monomeric and dimeric forms) CD spectra. The concentrations of proteins were 5 – 8 μM in OG and ~1μM in vesicles.

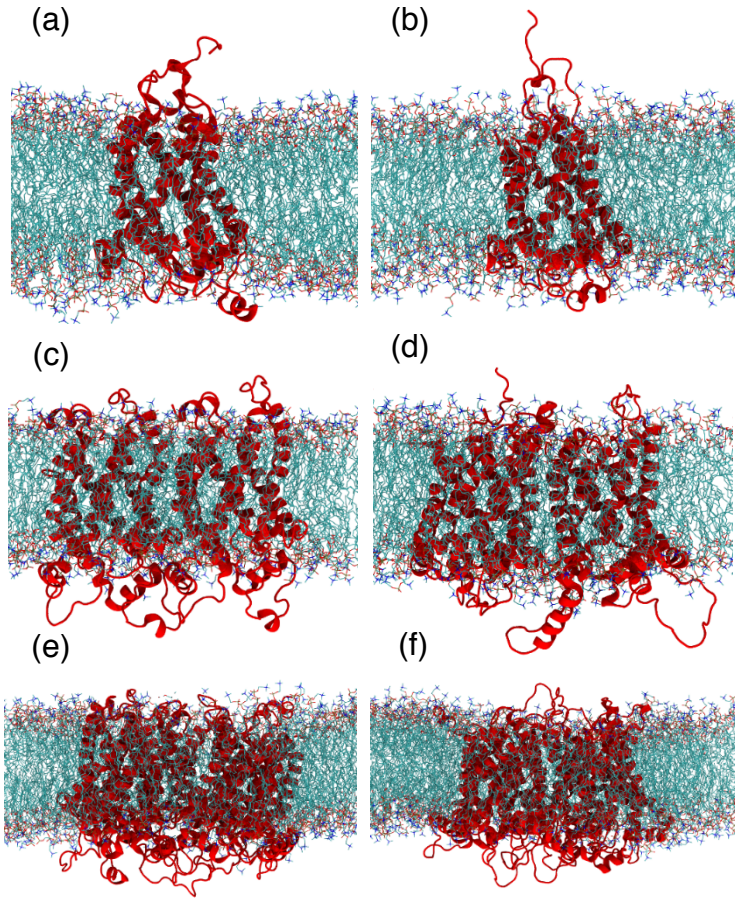

Figure 7. Initial (0 ns) and final (150 ns) MD structures of monomeric (a – b), dimeric (c – d), and tetrameric UCP2 (e – f). UCP2 shrinks in POPC bilayer during the MD simulation in all three forms. Monomeric UCP2 maintains its overall initial structure, tetrameric UCP2 adopts a more stable densely packed structure through interactions between the protein units and with the bilayer (Figures S7 – S9) while dimeric UCP2 undergoes more significant deformations (Figure S5). Overall, the MD simulation results suggest that UCP2 is stable in lipid bilayers and can potentially co-exist in monomeric and tetrameric forms. Compared to the monomeric (and dimeric) UCP2, the tetramer is structurally more stabilized in the bilayer.

Supporting Information

The role of matrix-oriented salt-bridge on the proton transport in a multimeric uncoupling protein 2

Afshan Ardalan[1], Stephanie O. Uwumarenogie[1], Michael Fish[1,2], Shahin Sowlati-Hashjin[3], Mikko Karttunen[3,4], Matthew D. Smith[2], and Masoud Jelokhani-Niaraki[1]*

[1] Department of Chemistry and Biochemistry, Wilfrid Laurier University, Waterloo, ON, Canada N2L 3C5
[2] Department of Biology, Wilfrid Laurier University, Waterloo, ON, Canada N2L 3C5
[3] Department of Chemistry, Western University, London, ON, Canada N6A 5B7
[4] Department of Applied Mathematics, Western University, London, ON, Canada N6A 5B7

Table of Contents

Figure S1.	Representation of the matrix salt-bridge network of UCP2 and its mutants	S-2
Figure S2.	Western blot analysis of AAC1	S-3
Figure S3.	Rate of proton transport by fluorescence quenching assay	S-3
Figure S4.	Projection of the MD simulation trajectories on the first 4 eigenvectors	S-4
Figure S5.	Backbone RMSD of UCP2	S-5
Figure S6.	RMSF of Cα of UCP2	S-5
Figure S7.	Salt-bridges between the neighboring UCP2 units	S-6
Figure S8.	Average number of hydrogen bonds in UCP2	S-7
Figure S9.	Average number of hydrogen bonds between UCP2 and lipid	S-8
Figure S10.	Radius of gyration of UCP2	S-9
Figure S11.	Overlay of the monomer final MD structure with the initial structure	S-9
Figure S12.	Overlay of the dimer final MD structure with the initial structure	S-10
Figure S13.	Overlay of the tetramer final MD structure with the initial structure	S-11
Figure S14.	Overlay of the dimer units with the initial structure	S-12
Figure S15.	Overlay of the tetramer units with the initial structure	S-13
Figure S16.	Solvent accessible surface area (SASA) of UCP2	S-14
Figure S17.	Superimposed structures of the matrix salt bridges in UCP2	S-15
Figure S18.	Representation of GXXXG motifs on UCP2 structure	S-16
Figure S19.	The GXXXG motifs in the structures of dimeric and tetrameric UCP2	S-16

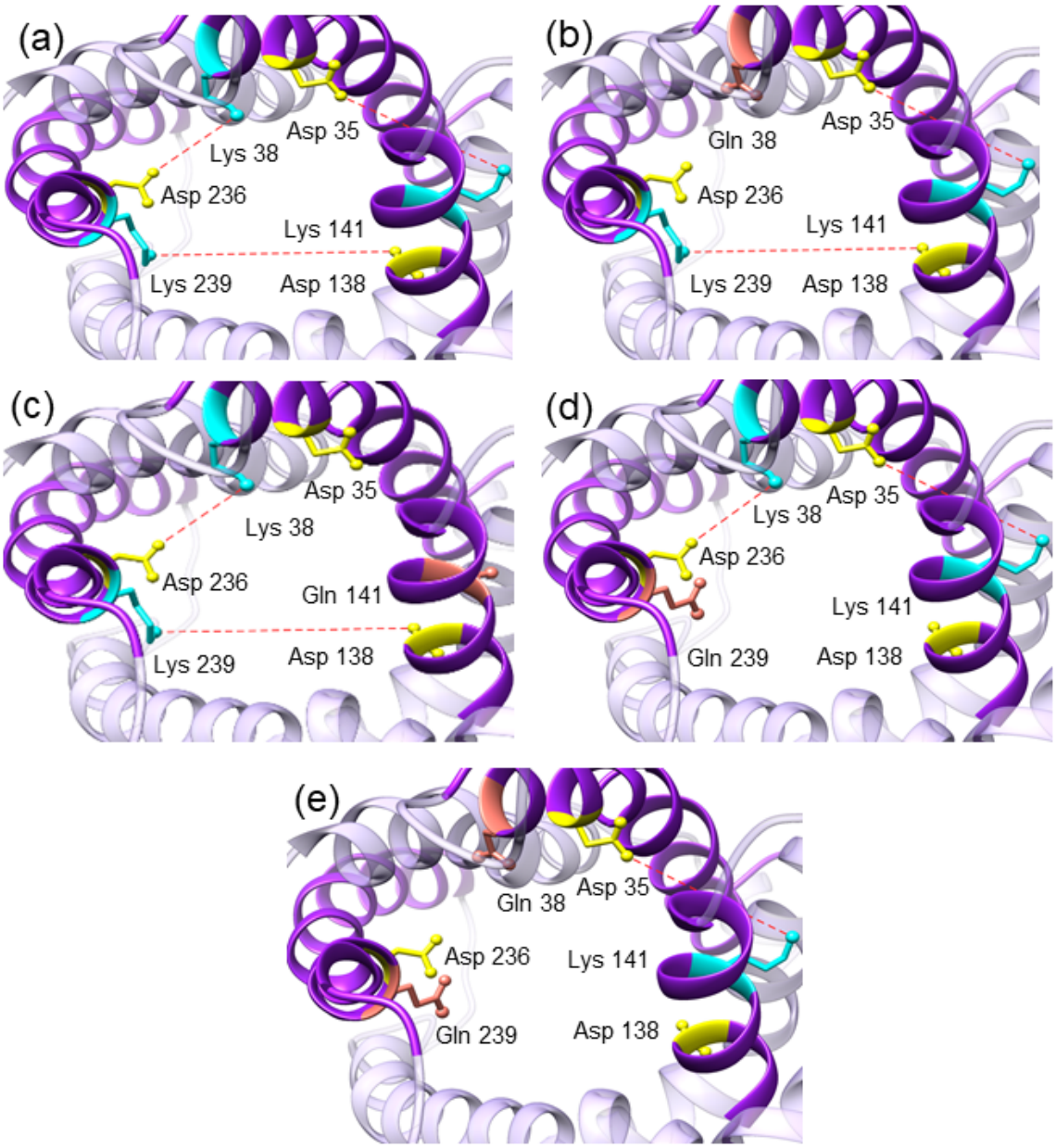

Figure S1. Representation of the matrix salt-bridge network of UCP2 and its mutants from the matrix side. (a) UCP2 (b) K38Q (c) K141Q (d) K239Q (e) K38Q/K239Q. The transmembrane domains 1, 3 and 5 are shown in dark purple. The transmembrane domains 2, 4 and 5 are pale purple. Lysine residues are shown in cyan, Aspartates are shown in yellow and glutamines in orange.

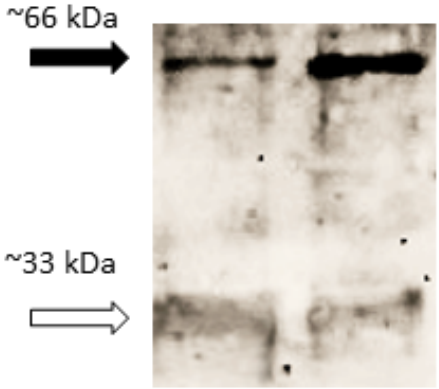

Figure S2. Western blot analysis of AAC1 probed with α-AAC1 antibody confirms the co-presence of monomeric and dimeric states in OG.

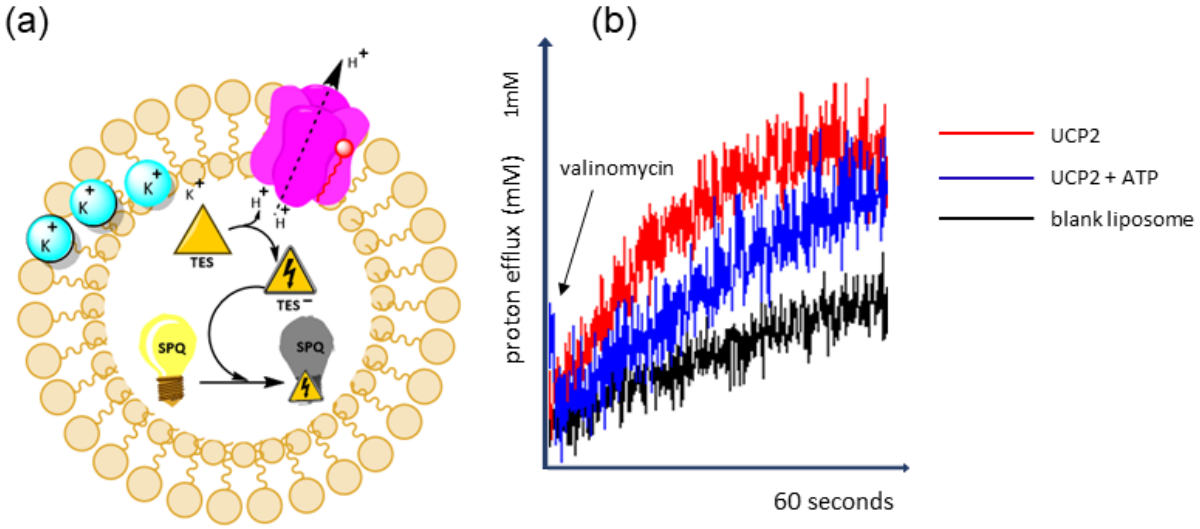

Figure S3. (a) Schematic view of the prepared proteoliposome for measuring the rate of proton transport by fluorescence quenching assay. The trapped SPQ fluorescent dye inside the vesicles can be quenched by TES^- anions. TES^- anions are generated as a consequence of increase in internal pH. Valinomycin directs the potassium ions into the liposomes resulting in an uneven charge distribution (inside positive) and osmotic imbalance across the lipid bilayer, which causes a fatty acid-dependent UCP2-mediated proton efflux. Thus, the rate of proton transport is indirectly measured by the rate of quenching of the SPQs fluorescence signal. (b) UCP mediated Proton transport in the absence and presence of ATP, and non-specific proton flux are shown for comparison.

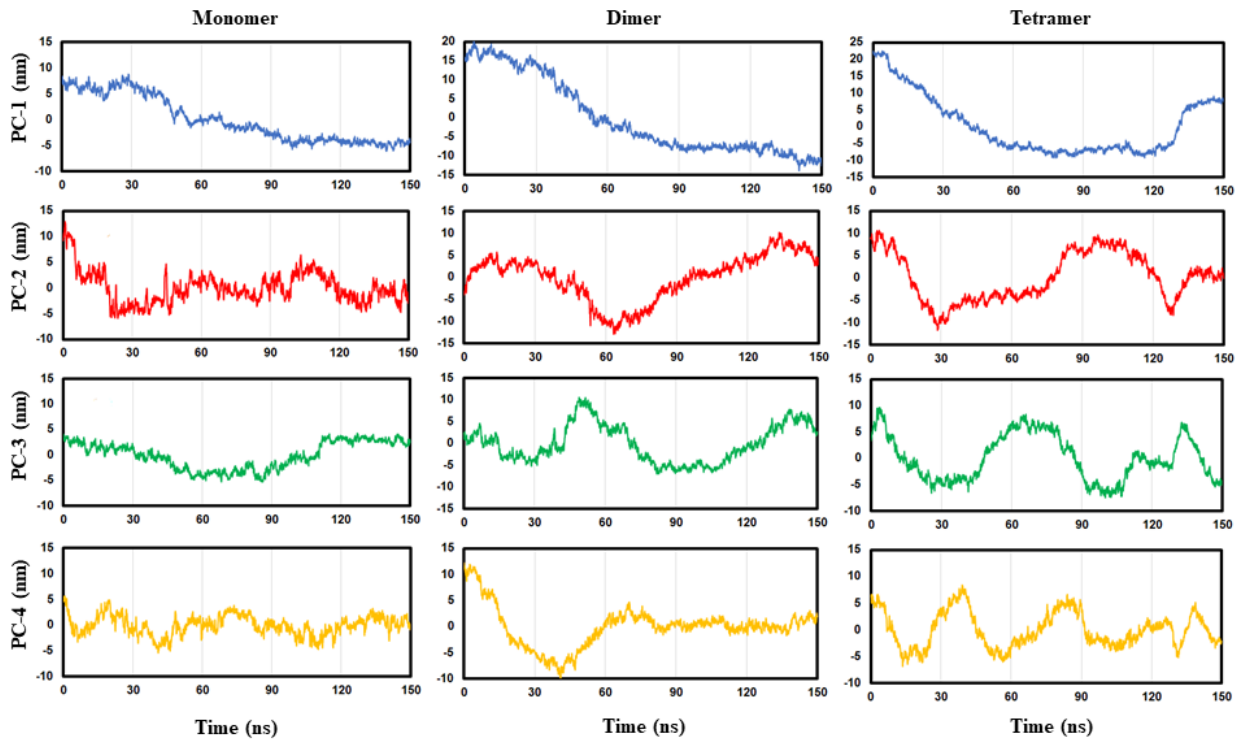

Figure S4. Projection of the MD simulation trajectories on the first 4 eigenvectors (principal component, PC) for monomeric, dimeric, and tetrameric UCP2 in POPC bilayer.

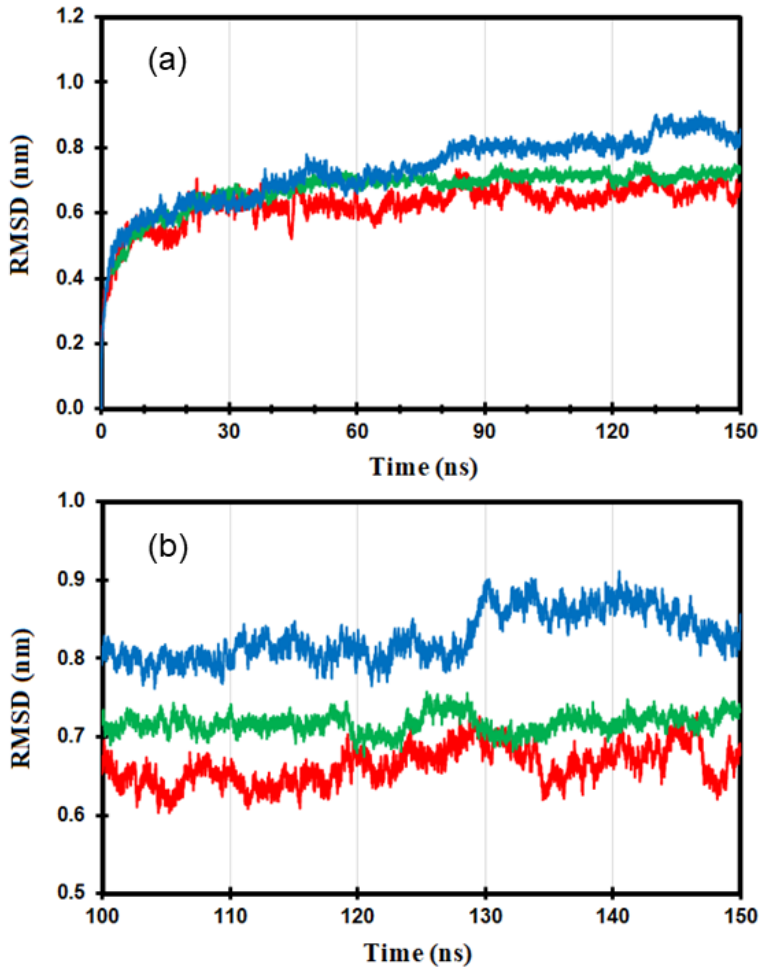

Figure S5. Backbone RMSD of monomeric (red), dimeric (blue), and tetrameric (green) UCP2 in the membrane (a) over the course of MD simulation and (b) the last 50 ns.

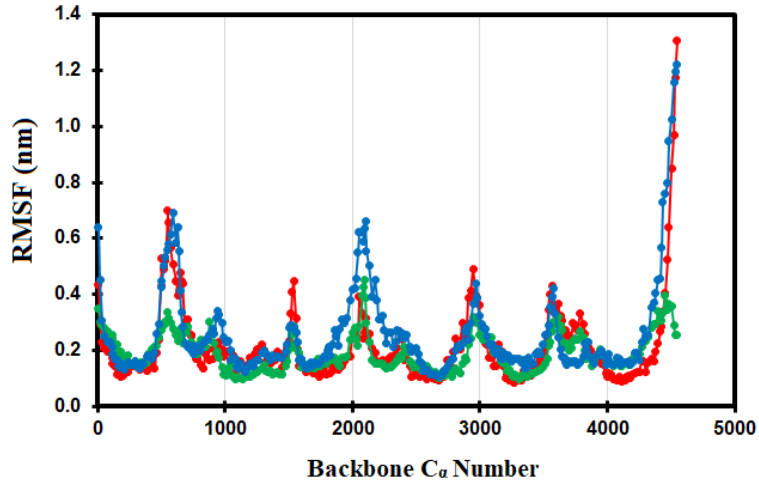

Figure S6. RMSF of C_α of protein for monomeric (red), dimeric (blue), and tetrameric (green) UCP2 in the membrane over the course of MD simulation.

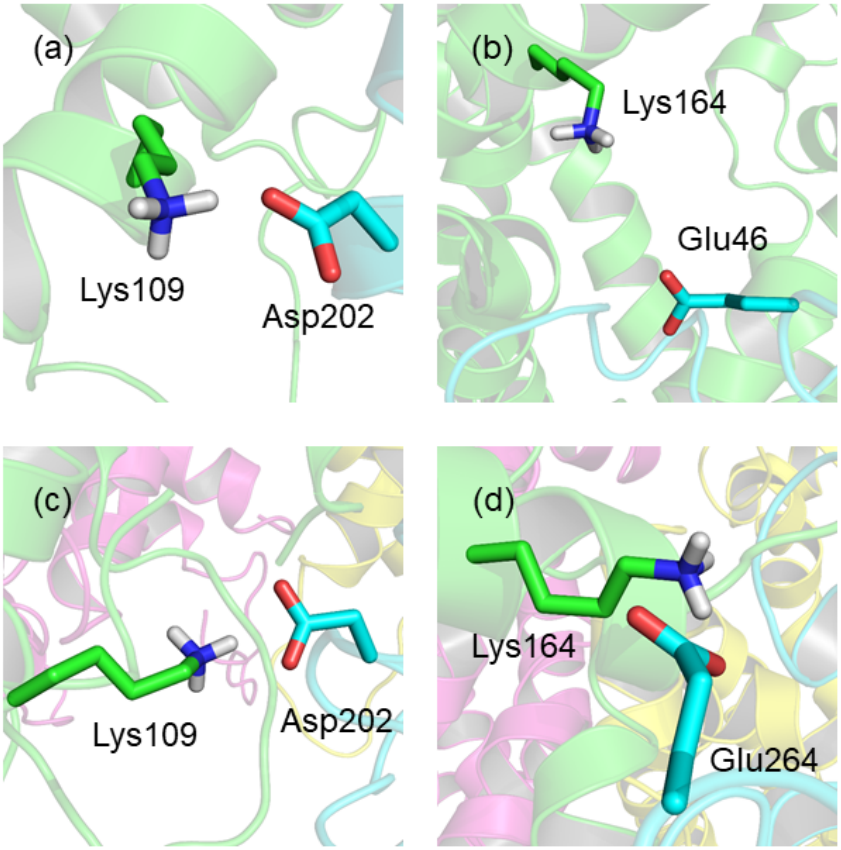

Figure S7. Salt-bridges between the neighboring UCP2 units in dimeric (a – b) and in tetrameric (c – d).

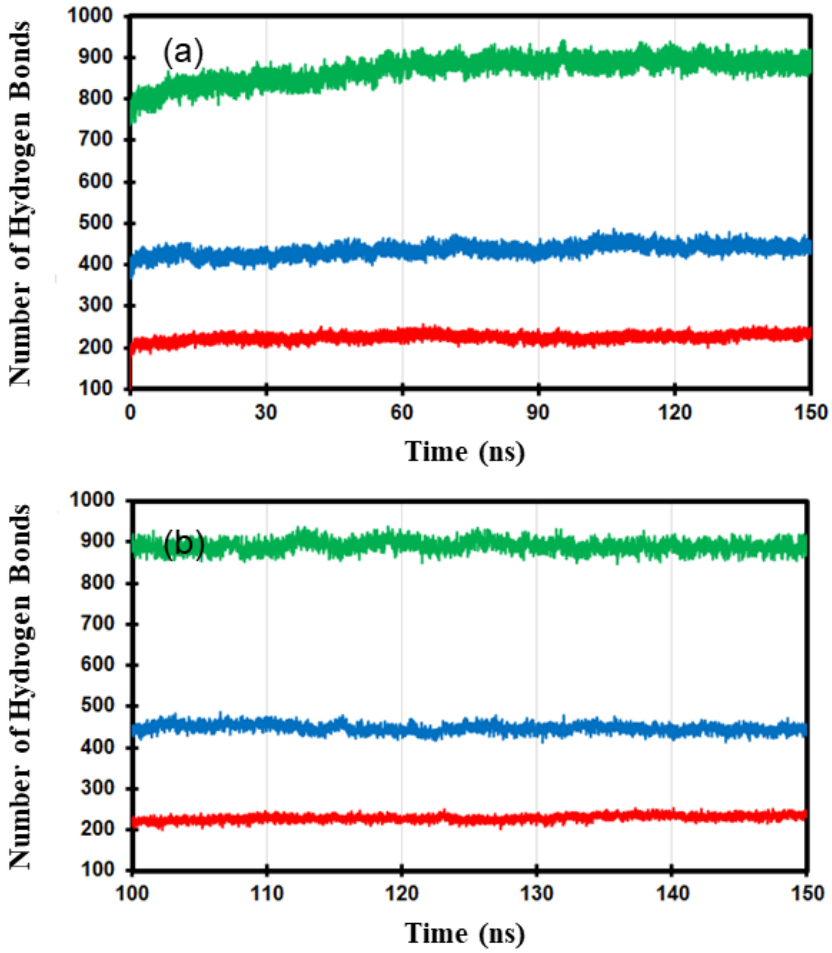

Figure S8. Average number of hydrogen bonds in monomeric (red), dimeric (blue), and tetrameric (green) UCP2 in the membrane (a) over the course of MD simulation and (b) the last 50 ns.

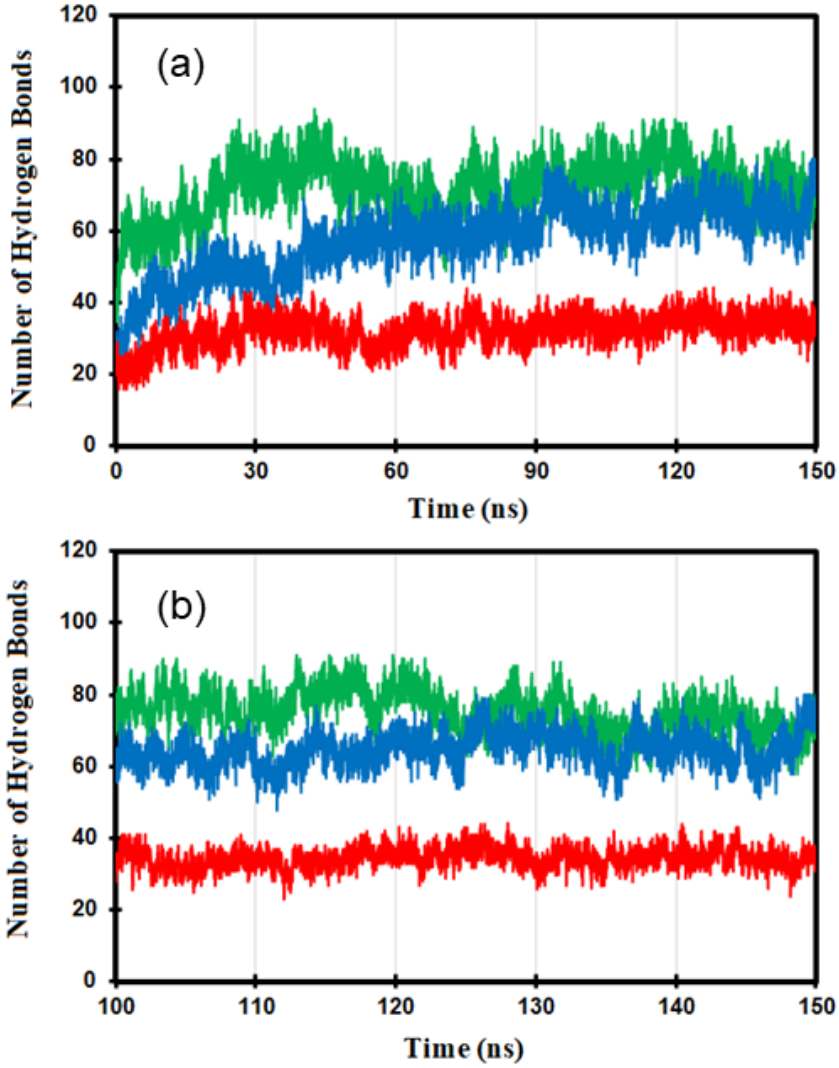

Figure S9. Average number of hydrogen bonds between UCP2 and membrane for the monomeric (red), dimeric (blue), and tetrameric (green) UCP2 (a) over the course of MD simulation and (b) the last 50 ns.

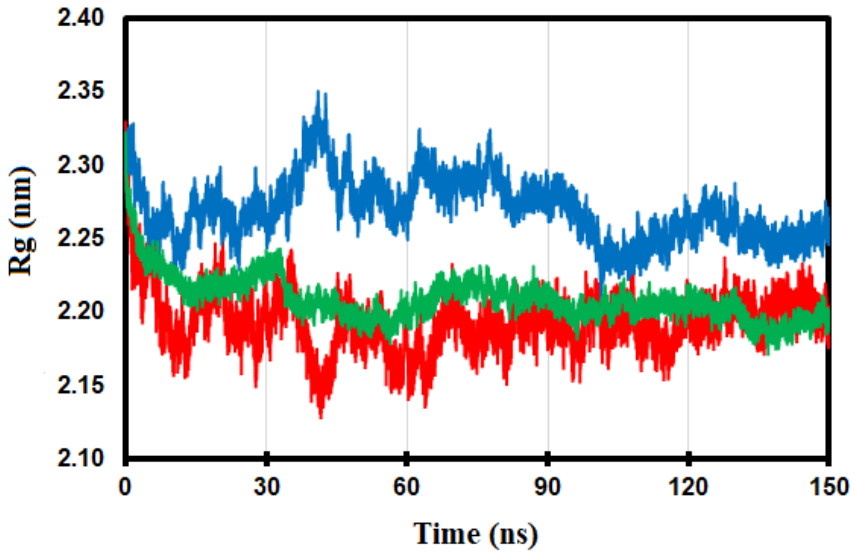

Figure S10. Radius of gyration for the monomeric (red), dimeric (blue), and tetrameric (green) UCP2 in the membrane over the course of MD simulation.

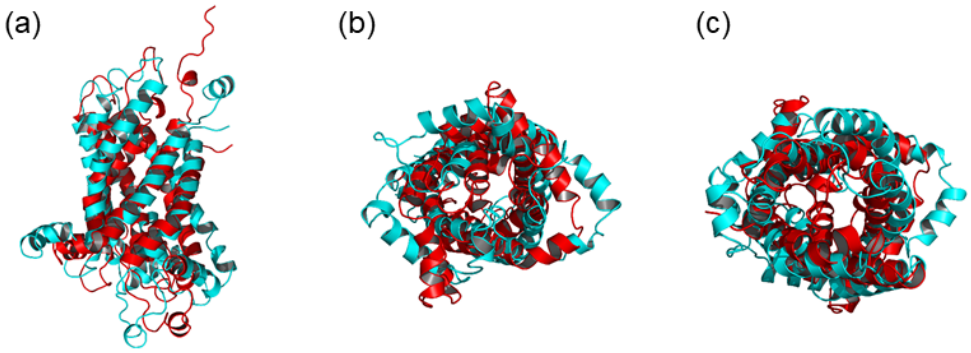

Figure S11. Overlay of the monomer final MD structure (red) with the initial structure (PDB ID: 2LCK, cyan) along (a) x-axis, (b) z-axis (top view), and (c) z-axis (bottom view).

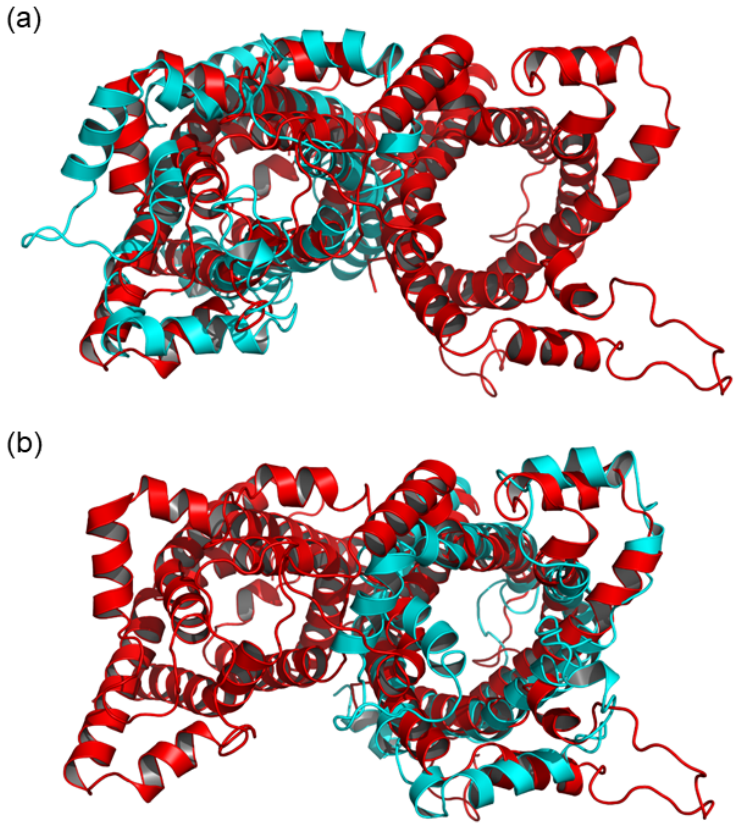

Figure S12. Overlay of the dimer final MD structure (red) with the initial structure (PDB ID: 2LCK, cyan).

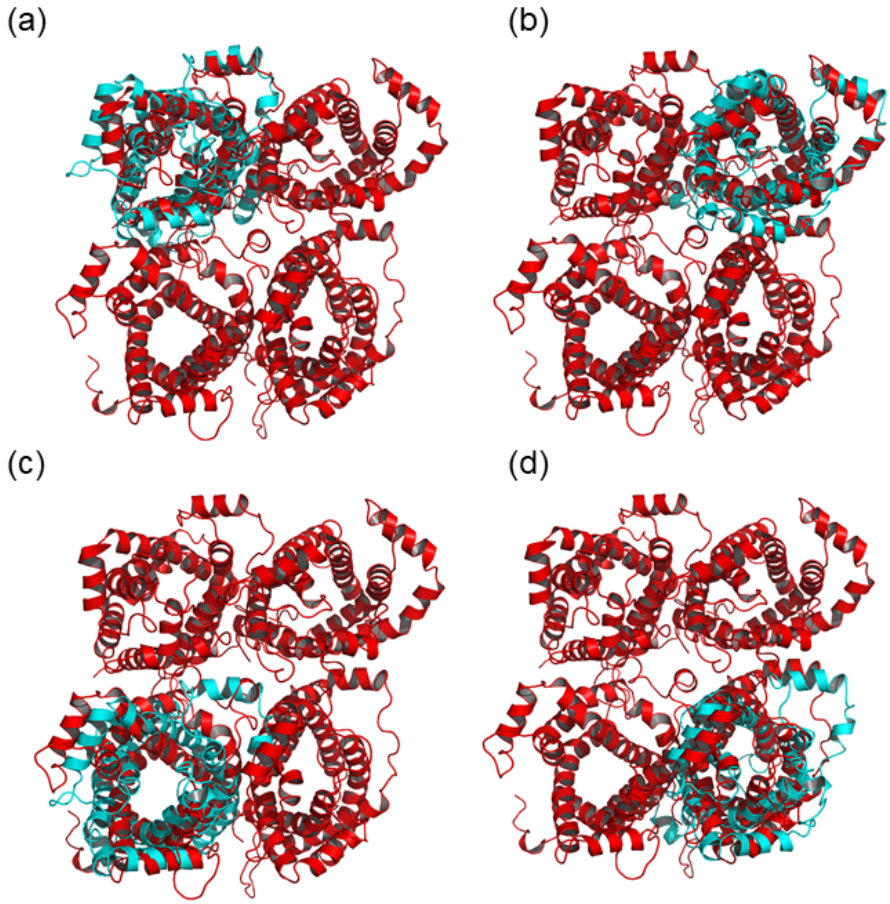

Figure S13. Overlay of the tetramer final MD structure (red) with the initial structure (PDB ID: 2LCK, cyan).

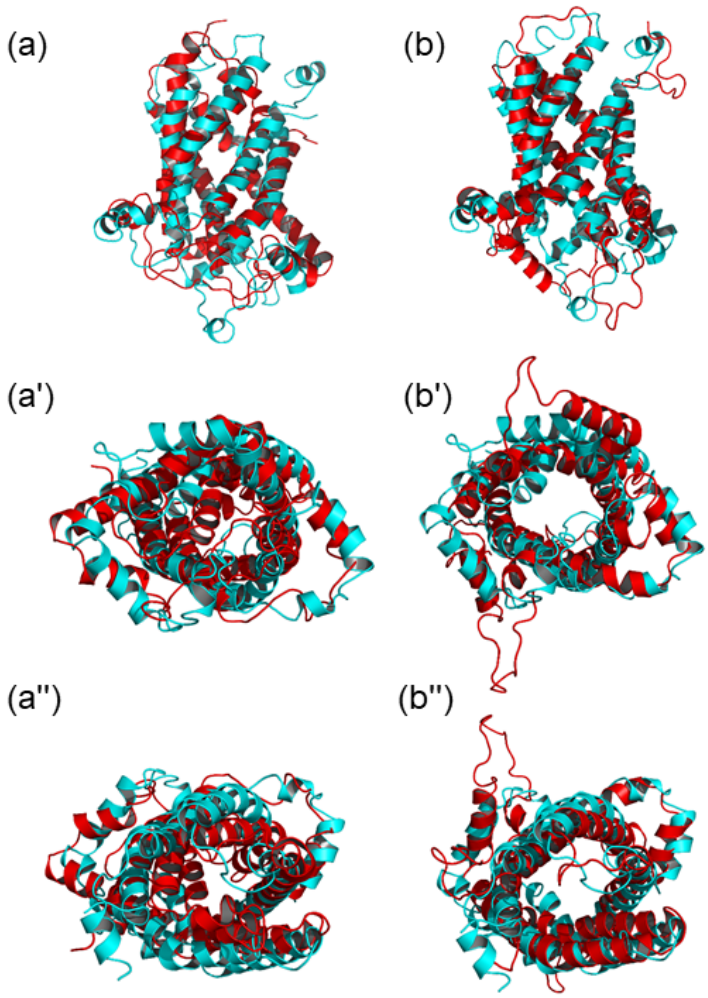

Figure S14. Overlay of the final MD structure of dimer units (red) with the initial structure (PDB ID: 2LCK, cyan) along (a – b) x-axis, (a′ – b′) z-axis (top view), and (c – c′) z-axis (bottom view).

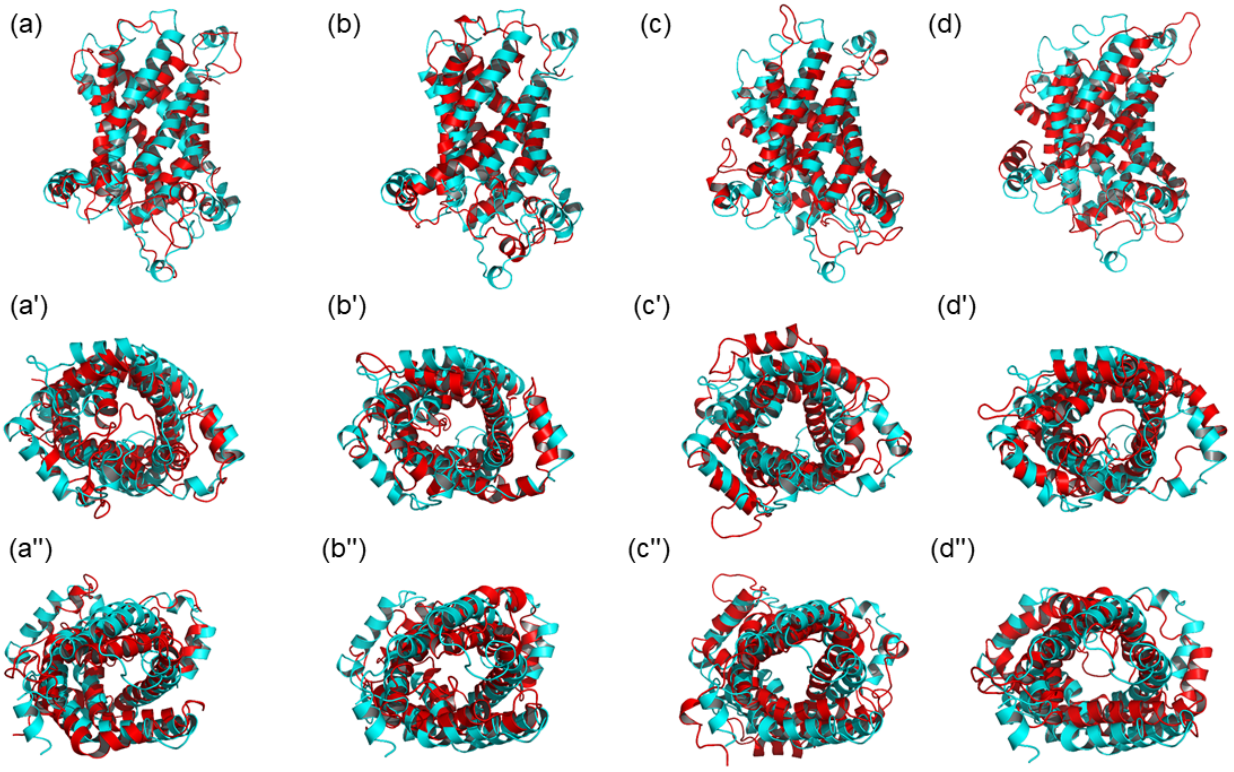

Figure S15. Overlay of the final MD structure of tetramer units (red) with the initial structure (PDB ID: 2LCK, cyan) along (a - d) x-axis, (a′ - d′) z-axis (top view), and (a″ - d″) z-axis (bottom view).

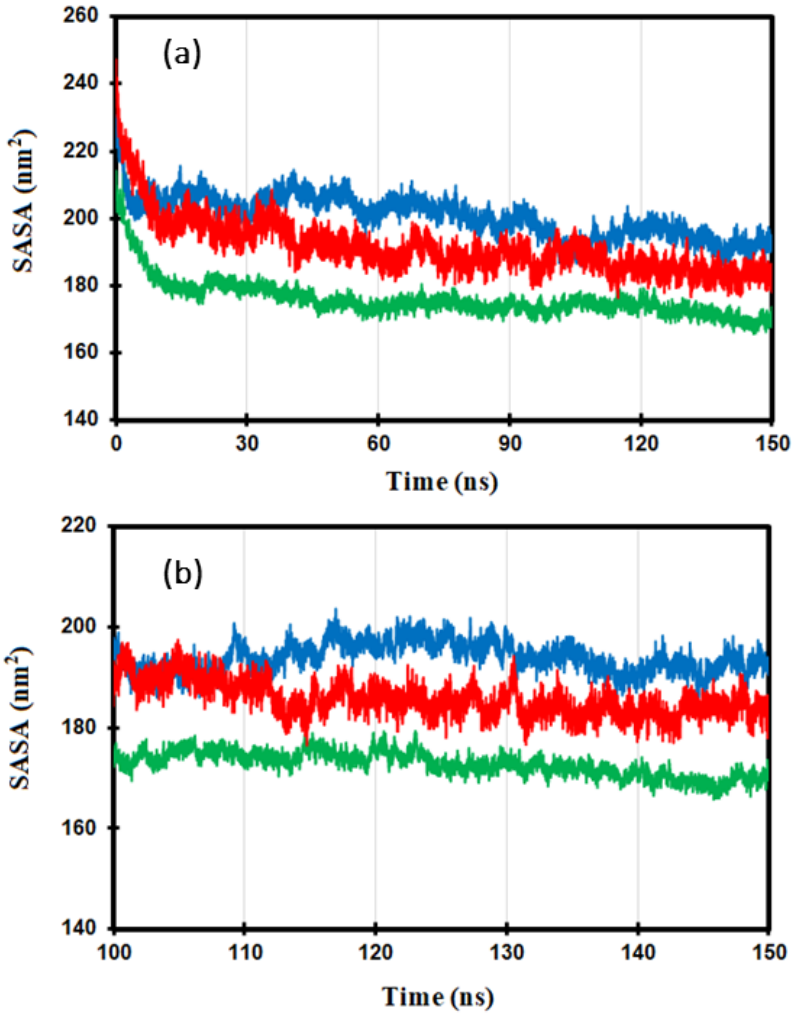

Figure S16. Solvent accessible surface area (SASA) of monomeric (red), dimeric (blue), and tetrameric (green) UCP2 in the membrane (a) over the course of MD simulation and (b) the last 50 ns.

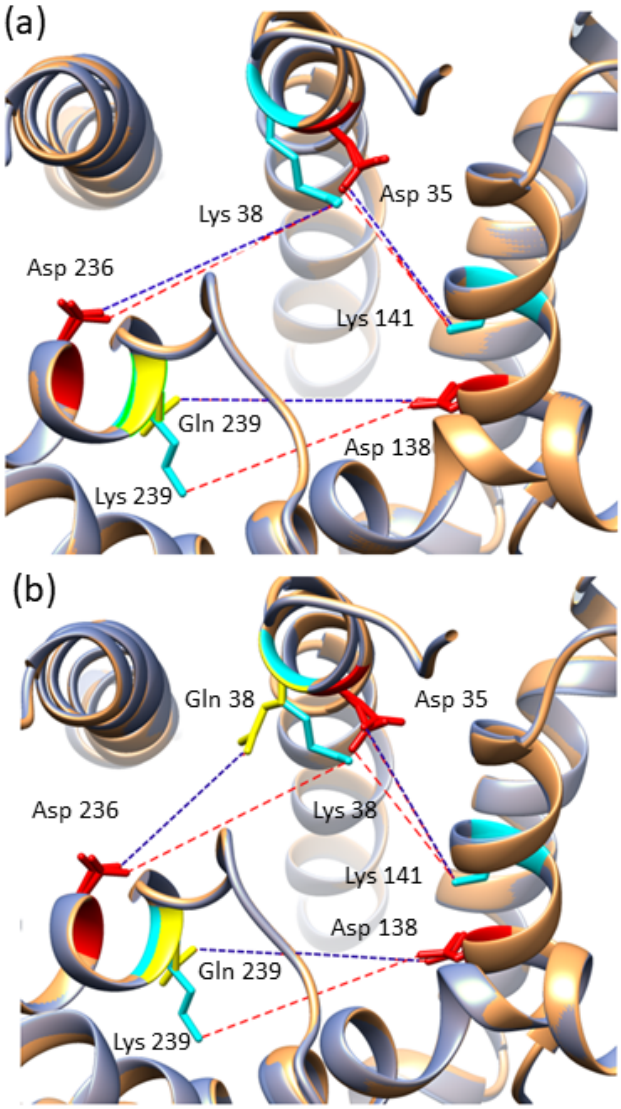

Figure S17. Superimposed structures of the matrix salt bridges in UCP2 and two of the mutants. (a) Superimposed structure of UCP2 and K239Q mutant as a presenter of the local changes in single mutations. (b) Superimposed structure of UCP2 and K38Q/K239Q mutant as a presenter of the local changes in double mutation**.** The superimposed structures are all based on one of the fifteen available snapshots of the UCP2 in NMR. The structures of the mutants are generated and minimized over a 1000 step minimization of the steepest decent method. UCP2 backbone: sandy brown, mutant backbone: light purple, aspartate: red, lysine: cyan, glutamine: yellow. The distances between salt bridge forming residues in UCP2: red. The distances between salt bridge forming residues/mutations in mutants: dark blue.

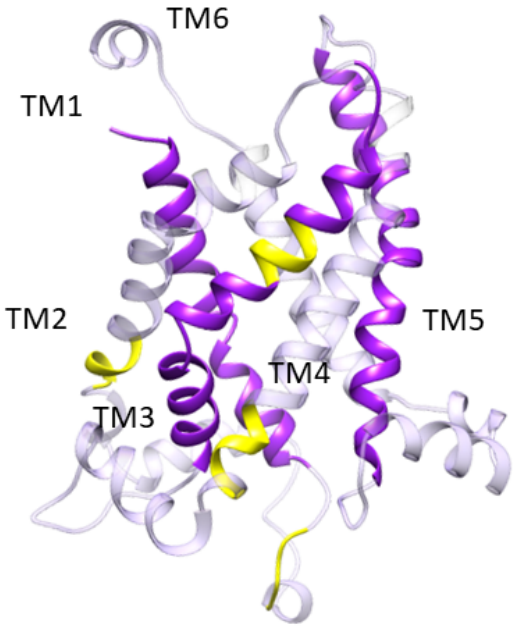

Figure S18. Representation of GXXXG motifs on UCP2 structure. GXXXG motifs are colored in yellow. Three out of four GXXXG motifs are present on one side of the protein on transmembrane domains (TM) 2, 3, and 4. This suggests a probable role for protein-protein interactions in oligomerization of UCP2. Transmembrane domains: 1, 3, and 5 dark purple. Transmembrane domains 2, 4, and 5: pale purple.

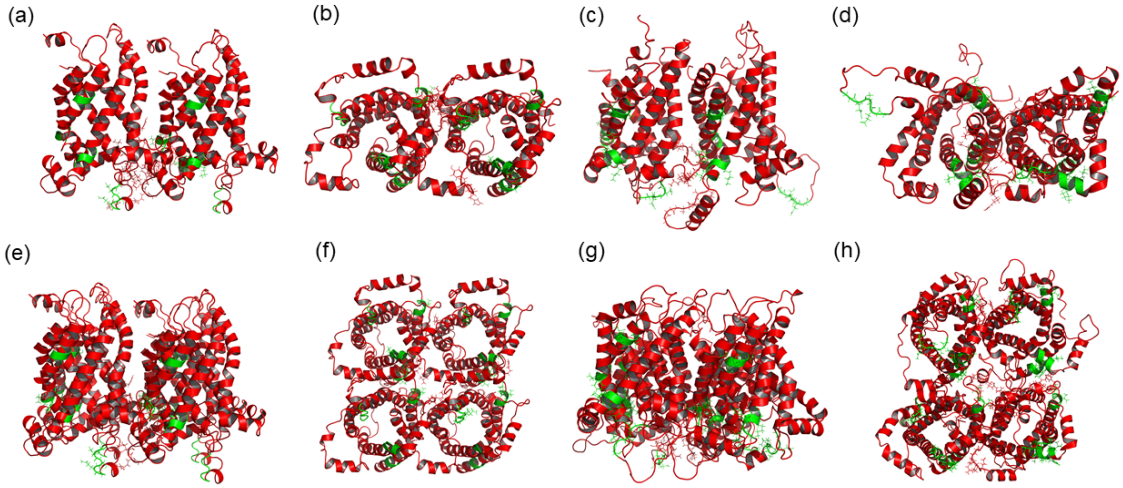

Figure S19. The GXXXG motifs (green) in the initial (a – b) and final (c – d) structures of dimeric UCP2 and in the initial (e – f) and final (g – h) structures of tetrameric UCP2.